Mon. Not. R. Astron. Soc. **294,** 1–27 (1998)

The APM survey for cool carbon stars in the Galactic halo – I

E. J. Totten[1,2] and M. J. Irwin[2]

[1]*Department of Pure and Applied Physics, The Queen's University of Belfast, Belfast BT7 1NN*
[2]*Royal Greenwich Observatory, Madingley Road, Cambridge CB3 0EZ*

Accepted 1997 July 29. Received 1997 June 30; in original form 1997 March 3

ABSTRACT

A by-product of the APM high-redshift quasar survey was the discovery of several distant (20–100 kpc) N-type carbon stars at high galactic latitude. Following on from this, we have started a systematic all-sky survey at galactic latitudes $|b| > 30°$ to find further examples of these rare objects, and we report here on the results from the first season of follow-up spectroscopy. Faint, high-latitude carbon (FHLC) giants make excellent probes of the kinematic structure of the outer Galactic halo. Therefore, in addition to detailed spectrophotometry covering a wide wavelength range, we have obtained high-resolution (~ 1 Å) spectra centred on the CN bands at ~ 8000 Å, and have derived accurate ($\lesssim 10$ km s^{-1}) radial velocities for the known FHLC stars. From the initial phase of our survey covering ≈ 6500 deg^2, we find a surface density of faint N-type carbon stars in the halo of ≈ 1 per 200 deg^2, roughly a factor of 4 less than the surface density of CH-type carbon stars in the halo. Intermediate-age, N-type carbon stars seem unlikely to have formed in the halo in isolation from other star-forming regions, and one possibility that we are investigating is that they either arise from the disruption of tidally captured dwarf satellite galaxies or are a manifestation of the long-sought optical component of the Magellanic Stream.

Key words: surveys – stars: carbon – Galaxy: formation – Galaxy: halo.

1 INTRODUCTION

Most known carbon stars are high-luminosity giants. With their characteristic spectra and distinct optical and near-infrared colours they can readily be detected out to large distances in the Galactic halo. Although the surface density of faint, high-latitude carbon (FHLC) stars in the halo is low (≈ 1 per 50 deg^2; Green et al. 1994), there seem to be at least three kinds of halo carbon stars present.

(i) The normal asymptotic giant branch (AGB) stars, carbon-enriched by dredge-up during the post-main-sequence phase, are found among the so-called N-type carbon stars. These intermediate-age stars are abundant in the Magellanic Clouds and are present in most of the Galactic dwarf satellite galaxies (Azzopardi & Lequeux 1992). Although there appears to be some dependence of absolute luminosity of the N-type carbon stars with age in the Galactic satellite galaxies, the majority have absolute magnitudes $M_R \approx -3.5$ and hence can be detected to very large distances (> 100 kpc).

(ii) The first-generation old carbon stars of the Galactic halo of ~ 0.8 M$_\odot$ are not thought to undergo carbon-enriched dredge-up, and the existence of the CH-type carbon star component, which forms the majority of the halo carbon star population, has been ascribed to mass transfer in binary systems (McClure 1979). These CH-type carbon stars are similar to the metal-poor carbon stars found in globular clusters (Harding 1962) and in some dwarf spheroidal (dSph) galaxies, and hence most are probably giants with absolute magnitudes $M_V \approx -2.5$.

(iii) A number of FHLC stars have been found to show significant proper motion, and are now believed to have the luminosity of a main-sequence dwarf (see Deutsch 1994 for a recent summary). Although these dwarf carbon stars mimic the overall spectral signature of giant carbon stars, they are distinguishable through their relatively high proper motion and apparently anomalous *JHK* infrared colours (e.g. Green et al. 1992). Dwarf carbon stars are thought to be in binary systems in which the main-sequence dwarf received material from the now-invisible companion during the ascent of the latter up to the AGB (Dahn et al. 1977).

However, this simple age dichotomy has been challenged by the discovery of massive, apparently relatively young (~ 1 Gyr), CH-type carbon stars in the LMC (Hartwick & Cowley 1991; Feast & Whitelock 1992), and it is possible that at least some of the CH-type carbon stars in the halo are similar to these LMC carbons. Likewise, some of the CH-type carbon stars found in the dSphs may be intermediate-age AGB carbon stars, rather than old, metal-poor stars.

Before the APM survey work there were only a few published FHLC stars known (e.g. Sanduleak & Pesch 1982; Margon et al. 1984; Mould et al. 1985; Bothun et al. 1991), and there has been considerable speculation as to their origin (e.g. Sanduleak 1980; van den Begh & Lafontaine 1984). These previously published FHLC stars are a mixture of dwarf, CH-type and N-type carbon stars. Their properties are summarized in Table 1.[1] The intermediate-age (1–7 Gyr), N-type AGB carbon stars are rarely seen at high galactic latitudes, and the distant ones seem unlikely to have formed in the halo in isolation from other star-forming regions, so how did they get there? One possibility that we are investigating is that they either arise from the disruption of tidally captured dwarf satellite galaxies or are a manifestation of the long-sought optical component of the Magellanic Stream. Lack of proper motion rules out the possibility of most of them being dwarf carbon stars (e.g. Green et al. 1991; Warren et al. 1992; Deutsch 1994); indeed, no faint N-type carbon stars have yet been shown to be dwarf carbon stars. Optical spectroscopy and *JHK* photometry confirms their carbon star type (they are indistinguishable from cool AGB carbon stars in nearby dwarf galaxies) and hence probable large distances.

Since only a small number of FHLC stars are known, more examples are urgently needed to shed light on these issues and to investigate the dynamical nature of the Galactic halo. If the majority of FHLC stars are giants, then they can be readily detected out to distances beyond 100 kpc and thereby form a set of tracers of the distant gravitational potential of the Galaxy. Moreover, the spatial distribution of the carbon stars provides a probe of the morphological structure of the Galactic halo to distances at least as large as those provided by either globular clusters or RR Lyrae stars (e.g. Saha 1985). Perhaps more importantly, the presence of significant numbers of intermediate-age carbon stars supports the conjectures of Searle & Zinn (1978) and Rodgers & Paltoglou (1984), whereby the Galactic halo has been contaminated by debris from previous tidal disruption, or mergers, of satellite dwarf galaxies.

In the remainder of this paper we expand upon some of these points, summarize previous surveys for FHLC stars, and describe and present results from a new survey specifically designed to find FHLC stars. Our ultimate aim is to cover all the high galactic latitude sky, $|b| > 30°$ (i.e., 20 000 deg^2). Here we present preliminary results obtained during the first observing season, from candidates selected from some 6500 deg^2 of sky in the south and north Galactic cap (SGC, NGC) regions and from studies of previously known FHLC stars. We have obtained both accurate radial velocities (5–10 km s^{-1} precision) and good signal-to-noise ratio fluxed spectra for all the carbon stars meeting our survey criteria. This will enable us to investigate their kinematics, true spatial distribution and carbon type, and hence their possible origin. Even in the event that all these objects are somehow an integral part of the Galactic halo, their velocities and large distances will enable direct studies of the velocity ellipsoid and rotation of the outer halo (e.g. Green et al. 1994).

[1]Here and throughout this paper we generally define a FHLC star as having an R-band magnitude $R \gtrsim 11$, equivalent to $V \gtrsim 12.5$ or $B \gtrsim 14$, and a galactic latitude $|b| \gtrsim 30°$. For completeness, we have also included a few well-known FHLC stars brighter than this limit.

2 BACKGROUND

Characteristic time-scales for galaxy–galaxy interactions are much shorter than a Hubble time, and therefore interactions between galaxies are of vital importance for their evolution. Current models of galaxy formation imply that a galaxy like the Milky Way grew initially from a high primordial density fluctuation, on to which there merged over time the evolutionary results of a large number of smaller density fluctuations (e.g. Searle & Zinn 1978). In this picture typical 1σ fluctuations gave rise to dwarf-galaxy-sized perturbations which either evolved into dwarf galaxies or were incorporated into the Milky Way. Capture time-scales for tidal interaction are $\propto M^{-1}$, where M is the mass of the captured galaxy, suggesting that after an initial rapid growth subsequent capture and integration of progressively smaller systems takes place over a Hubble time. In the Milky Way the presence of a thin disc rules out large merging events in recent times, but many minor mergers, such as those with dwarf spheroidal satellites, are allowed (e.g. Unavane, Wyse & Gilmore 1996). The many studies of the LMC/SMC (and the Magellanic Stream), which is a prototypical system in the intermediate stages of tidal disruption, and also the recent discovery of the Sagittarius dwarf galaxy (Ibata, Gilmore & Irwin 1994) in the late stages of disruption prior to incorporation by the Galaxy support this view.

A consequence of this scenario is that disrupted satellites should leave a trail of debris tracing out their original orbital path before final disruption. Various numerical studies (e.g. Oh, Lin & Aarseth 1995) have shown that disruption of a satellite galaxy proceeds by the formation of a leading tidal bridge and a trailing tidal tail that follow the original orbital path of the satellite. After significant tidal disruption at a perigalactic passage, disintegration is rapid and, even over one orbit, leads to an enormous elongation of the dwarf along the orbital direction. Lateral spreading proceeds more slowly such that in principle it is still possible to trace the original Great Circle path of the original orbit after several passages (Johnston et al. 1996). A typical satellite galaxy has an orbital period ≈ 1 Gyr, and so we might still expect to find coherent traces of dwarf galaxies captured several Gyr ago. Unfortunately, the lateral velocity dispersion of ≈ 10 km s^{-1} causes any stellar debris to spread rapidly (~ 1 Gyr) over several degrees, or more, of sky, making it hard to find by direct searches. Indeed, nearly two-thirds of the sky has already been thoroughly searched for Galactic dwarf satellite galaxies using a combination of techniques (Irwin 1993), including 'serendipitous' searches

for moving groups. It is highly unlikely that more than a few intact dwarf satellites are left to be discovered, and the number of unknown dwarf galaxies in the early stage of disruption must also be small, since direct morphological traces of them would have been found.

Lynden-Bell (1976) suggested an alternative approach. The arc of the Great Circle formed by the Magellanic Stream crosses 120° of sky (Mathewson, Clearly & Murray 1974), and is sufficiently similar to the tidal arms studied by Toomre & Toomre (1972) that a tidal origin seems highly probable. The recent measurement of the proper motion of the LMC by Jones, Klemola & Lin (1994), showing that the Magellanic Streams trail along the orbital plane of the LMC, strongly supports this conjecture. The eventual accretion of the Magellanic Clouds via tidal friction appears inevitable (Tremaine 1976), suggesting that other distant small satellites and clusters of the Galaxy may be debris associated with mergers. Indeed, as noted by Kunkel & Demers (1976) and Lynden-Bell (1976), and more recently by Majewski (1994) and Lynden-Bell & Lynden-Bell (1995), several potential tidal streams of halo objects can be traced in the satellite population. However, dwarf-galaxy-sized fragments or globular clusters would not be the only easily traced remnants. All of the satellite galaxies in the Milky Way have cool AGB carbon star populations present. These objects are extremely rare in the outer Galactic halo, are redder than all other common Galactic stars, and are extremely easy to find using photographic surveys. This makes them ideal tracers of galaxy populations, disrupted or otherwise. If, for example, the Magellanic Stream has an optical counterpart, then finding its AGB carbon stars is possibly the best means of identifying it (e.g. Irwin 1991). Likewise, if a dwarf satellite galaxy were disrupted 1 Gyr or more ago, identifying its orbital comoving remnant carbon stars is an excellent method of finding and investigating it. By restricting our new survey to optically red colours, in addition to producing manageable numbers of candidates for follow-up spectroscopy, most of the carbon stars found ought to be N-type with only a small overlap in sensitivity to CH-type stars around spectral types M1–M2 and later (Keenan 1993).

The average absolute R-band magnitude of cool AGB carbon stars in the Magellanic Clouds is $M_R \approx -3.5$ (Kunkel, Demers & Irwin 1996). This is also consistent with the range of absolute magnitudes of the cool AGB carbon stars found in most of the dSph satellites (Azzopardi & Lequeux 1992). For example, Fornax, Leo I and Carina all have a substantial intermediate-age population with a well-defined AGB and a confirmed AGB carbon star content (Azzopardi & Lequeux 1992). Indeed, in all Local Group galaxies surveyed so far, carbon stars similar to those present in the Magellanic Clouds have been found in large numbers (Richer & Westerlund 1983; Azzopardi & Lequeux 1992). There is some correlation between the ages and luminosities of carbon stars, with Fornax having the youngest intermediate-age stars and the brightest carbon stars, but the ubiquitous presence of AGB carbon stars highlights their potential as tracers of disrupted systems. These carbon stars are intrinsically bright enough to be readily detectable out to Galactocentric distances of 100 kpc and beyond, and therefore provide an excellent probe for investigating phase-space structure in the outer halo.

3 PREVIOUS SURVEYS

The current status of searches for FHLC stars was summarized by Green et al. (1994). Most of the known FHLC stars were originally selected from two objective-prism surveys, the Case Low Dispersion northern sky survey (Sanduleak & Pesch 1988) and the University of Michigan Thin Prism survey (MacAlpine & Lewis 1978; Bothun et al. 1991). The Case survey covered ≈ 1000 deg^2 of the NGC, and the University of Michigan survey covered ≈ 225 deg^2 of the SGC. Both used hypersensitized Kodak IIIa-J plates which have a red wavelength cut-off of 5400 Å. Candidate carbon stars were generally recognized by the presence of the 4737- and 5165-Å Swan C_2 bands. However, the redder N-type carbon stars are often visible only redward of the 5165-Å absorption band, and their short stubby spectra are therefore hard to distinguish from those of other late-type stars. Consequently, N-type carbon stars are poorly represented in these IIIa-J plate surveys, which were mainly sensitive to the bluer CH-type carbon stars (see Table 1), and had an effective limiting magnitude of $V \approx 16$ for them (Green et al. 1994).

More recently, Green et al. (1994) conducted a CCD survey for FHLC stars, selecting candidates for further spectroscopic follow-up on the basis of two-colour photometry to a depth of roughly $V = 18$. In the 52 deg^2 surveyed only one highly ranked $V = 17$ candidate was found to have strong carbon features. This low apparent surface density ≈ 1 per 50 deg^2, is consistent with the paucity of FLHC stars uncovered during other less directed surveys. As the surface density of FHLC stars is so low, this suggests that photographic surveys are still the only practical means of finding significant numbers of them. This is particularly true for the N-type FHLC stars, where the surface density to $R = 17$, or equivalently $V = 18$, is ≈ 1 per 200 deg^2.

The Case and University of Michigan prism surveys, together with other prism surveys by Sanduleak & Philip (1977) and Westerlund et al. (1986), plus numerous other published carbon star samples, were compiled to make a single catalogue by Stephenson (1989). However, very few of the additional stars in Stephenson's catalogue are FLHC stars. Even with the more conservative selection criteria $V \gtrsim 12$ and $|b| \gtrsim 30°$, there are only a few additional candidates. In constructing Table 1, we have included, for completeness, all of the known dwarf carbon stars and the dusty carbon stars at high latitude found in the *IRAS* sky survey (Cutri et al. 1989; Beichmann et al. 1990). The FHLC stars are split into two groups; those that have been previously investigated in some detail are included, and those remaining from the Stephenson catalogue that require more detailed spectroscopy and photometry to ascertain their status have been omitted.

Many of the FHLC stars in Table 1 were serendipitous discoveries. Ironically, our own survey for carbon stars was stimulated by the success of the APM quasar survey in 'accidentally' discovering several faint, high-latitude N-type carbon stars. The APM[2] survey for high-redshift quasars, $z \gtrsim 4$, (Irwin, McMahon & Hazard 1991a) used UK Schmidt telescope (UKST) B_J and R sky survey plates to look for very red, $B_J - R > 2.5$ to 3.0, faint, $16 \lesssim R \lesssim 19$ candidate quasars. Brighter candidates, up to an R magnitude of $R \approx 12$, were

[2]The Automatic Plate Measuring facility in Cambridge.

Table 1. Previously published faint high-latitude carbon stars.

Ra	Dec	R	$B_J - R$	J	H	K	Vo(km/s)	Notes
								Dwarf Carbon Stars
00 23 29.3	−19 35 15	14		12.54	11.96	11.64	56	C*22, LHS1075 Green et al. 1991
00 41 08.1	−29 34 33	18.3	2.1	17.34[1]	16.39[1]	15.98[1]		Warren et al. 1993
00 45 50.5	−25 54 59	18.7	2.2					Warren et al. 1993
03 30 01.9	01 48 28	12.7	1.9	11.51	10.85	10.48	−34	G77-61 Dahn et al. 1977
08 24 01.8	28 53 57	13.5	0.7	12.72	12.15	11.93		dC+DA Heber et al. 1993
10 51 42.8	34 18 31	16.6	1.9	15.49	14.97	14.69	−44	CLS31(vr) Green et al. 1991
11 16 33.8	−16 28 24	14.4	1.7				−69	KA-2 Ratnatunga 1983
12 17 31.3	37 04 41	15.4	1.8	14.38	14.03	13.74	−167	CLS50(r) Green et al. 1992
15 17 33.4	50 17 51	16.8	0.4					CBS311 dC+DA Liebert et al 1994
15 50 36.4	29 37 01	14.9	2.1	13.75	13.14	12.82	+164	CLS96(r), LP328-57 Green et al. 1991
20 48 54.8	−34 48 51	18.7	2.6					Warren et al. 1992 dwarf ?
								Dusty Carbon Stars
08 54 37.0	17 32 27	19.9	>2	14.05	11.57	9.78		Cutri et al. 1989
12 56 04.7	16 56 23	15.9	>6	10.36	8.59	7.05		Beichman et al. 1990
								Normal? Carbon stars
00 02 51.2	00 53 22	12.9	1.7	11.00	10.38	10.16	+17	C*01
01 00 13.0	−16 19 08	14.5	1.3	13.13	12.57	12.51	−140	C*23
01 02 28.2	−05 56 08	15.3	2.8	11.11	9.89	8.71	+21	C*07 + APM
01 08 51.1	−00 15 54	15.1	1.5	13.47	12.81	12.75	−143	C*03
02 07 39.6	−02 11 47	12.8	4.9	10.90	10.14	9.72	−131	C*30 + APM
02 17 49.0	00 56 57	13.4	2.9	10.96	10.08	9.73	−138	C*31 + APM
02 22 44.2	−13 37 31	9.0	2.0:	7.33	6.43	6.09	−11	C*15
02 28 43.9	−02 56 21	14.5	1.8	12.53	11.86	11.66	−72	C*08
02 29 49.5	−03 16 52	15.8	2.1	11.81	11.01	10.69	−128	C*09
03 11 44.1	07 33 37	15.7	1.8					Green et al. 1994
09 11 48.7	33 41 29	12.9	1.2	11.20	10.69	10.59	−59	CLS9(r)
09 39 46.0	36 30 45	14.5	1.1	13.45	12.95	12.90	+123	CLS14(y)
10 15 56.6	35 40 17	13.6	1.7	12.54	12.05	11.78	+100(47)	CLS23(r) Mould et al. 1985
10 25 01.0	29 23 17	13.3	1.7	12.15	11.71	11.62	+142	CLS26(y)
10 37 15.6	36 03 44	14.3	2.0	12.92	12.30	12.02	+23	CLS29(r) Mould et al. 1985
10 56 35.2	40 00 12	12.3	3.3					FBS1056+399 + APM
11 23 34.4	37 23 58	11.5	2.4	10.03	9.36	9.15	−24	CLS38(vr) + APM
11 30 52.3	−10 20 24	14.0	9.1				−24	Nguyen-Q-Rieu et al 1987 + APM
11 35 17.6	33 21 29	14.8	1.3	13.19	12.67	12.47	+5	CLS43(r) Mould et al. 1985
11 49 25.1	37 27 50	12.9	1.5	11.07	10.56	10.32	−178	CLS45(r) Mould et al. 1985
12 13 07.9	37 21 07	13.2	1.0	12.14	11.73	11.65	−27	CLS48(y)
12 31 55.1	36 25 59	11.8	1.8	9.79	9.14	8.92	−186	CLS54(vr) Mould et al. 1985
12 39 38.1	31 22 32	9.9	2.3	9.62	9.00	8.86	+60	CLS57(r) Mould et al. 1985
12 52 17.8	10 17 49	13.7	1.7	12.03	11.45	11.28	+45	Phillips & Terlevich 1983
13 13 14.3	35 35 41	14.1	1.5	12.19	11.61	11.38	+40	CLS67(r)
14 15 31.7	29 36 56	11.9	1.8	10.69	10.27	10.17	−217	CLS80(r)
15 09 46.7	−09 02 49	16.5	2.0	15.33	14.72	14.47	+75	Margon et al. 1984
15 23 53.3	42 35 18	14.5	4.8	9.93	8.85	7.86	+17	Sanduleak & Pesch 1982 + APM
15 25 48.6	29 12 28	15.0	2.1	13.46	12.89	12.70	−25	CLS87(r)
15 32 59.8	32 42 16	13.9	1.6	11.85	11.21	10.97	−67	CLS90(vr)
16 05 47.7	29 22 41	12.6	1.9	10.67	10.16	9.99	−135	CLS98(r)
16 16 37.0	39 30 32	13.8	1.5					Kurtanidze 1996
16 37 29.6	34 37 13	14.0	1.9	12.43	11.98	11.83	−189	CLS105(r)
17 06 07.1	33 16 13	14.1	1.2	13.28	12.92	12.79	−58	CLS112(r)
17 12 37.4	42 03 50	13.0	1.7					Kurtanidze 1996
22 13 42.7	−14 51 24	13.9	2.1	11.96	11.29	11.03	0	C*26
23 05 09.0	−13 56 41	15.2	0.7	13.53	12.88	12.70		C*13 Wrong object ?
23 46 41.0	02 48 19	15.0	1.6	13.08	12.43	12.26	−143	Sanduleak 1980 + C*10
23 54 40.8	00 21 33	15.1	1.8	13.61	12.96	12.88	−72	C*02

Notes:
CLS stars are from the Case prism survey (Sanduleak & Pesce 1988), confirmed as carbon stars by Mould et al. (1985), Bothun et al. (1991) and Green et al. (1992). C*n are from Bothun et al. (1991). FBS is from the First Byurakan Survey (Abramyan & Gigoyan 1993). Magnitudes where possible are from the APM survey. Most of the FHLC stars in the table are CH-type; the confirmed N-type carbon stars C*07, C*30, C*31 and 1523+4235 are all selected by the APM survey, in addition to some of the redder CH-type (all denoted by +APM in the last column). The *JHK* photometry quoted uses the CIT/CTIO photometric system, except that [1] is from the AAT.

also routinely followed up spectroscopically, since there were so few of them. In addition to the high-redshift quasar population, the survey was also sensitive to late-type M stars, M7 or later (e.g. Irwin, McMahon & Reid 1991b) and, as it transpired, cool AGB carbon stars. The quasar survey covered ≈ 2500 deg^2 of high galactic latitude sky, and led to the discovery of a dozen or more distant (20–100 kpc) cool AGB carbon stars, all N-type. Other than the rediscoveries of previously known carbon stars, we defer listing the APM carbon stars until Table 3, since they have not been previously published and form part of our new APM survey.

4 THE APM SURVEY

The recent availability of APM object catalogues, derived from APM measures of red and blue sky survey plates covering most of the high-latitude sky (e.g. Irwin, Maddox & McMahon 1994), means that it is now feasible to extend the original APM survey to cover most of the high-latitude sky. In the south, in practice $\delta < 3°$, UKST sky survey plates in the so-called B_J and OR, or R, pass-bands form the raw plate material. In the north, in this case $\delta > -3°$ to allow some overlap for internal calibration of the survey, glass copies of Palomar sky Survey (POSS1) O and E plates are used, with the occasional, i.e., as available, new Palomar sky survey (POSS2) B_J and R copy plates thrown in for good measure. The effective wavelength regions covered by these survey plates are: $O \equiv 3400$–4900 Å; $B_J \equiv 3900$–5400 Å; $E \equiv 6200$–6900 Å; $OR \equiv 5900$–6900 Å; $R \equiv 6200$–6900 Å. The broad baseline provided by the $O-E$ or B_J-R colours makes the survey very sensitive to objects with extreme colours, such as the N-type carbon stars. The drawback is that most of the CH-type carbon stars lie too close to the main stellar locus to be reliably detected. However, since most of the previous large-area surveys were sensitive to mainly CH-type stars, the new APM survey can be thought of as complementing those searches, in addition to providing magnitude and colour estimates for previously known, or candidate, FHLC stars. Furthermore, by restricting the search to very red objects, the number of candidates is optimally minimized, and this makes it feasible to survey all of the high-latitude sky.

4.1 Plate measurement

The following points summarize the salient features of the APM measurements of the sky survey plates that provide the raw input needed for the carbon star survey (for more details see Kibblewhite et al. 1984, Irwin & McMahon 1992 and Irwin et al. 1994).

(i) The northern sky survey is mainly based on 6.2×6.2 deg^2 scans of glass copies of the POSS1 O and E sky survey plates taken in the 1950s. The field centres are on a 6° grid. The limiting magnitude is approximately 21.5 for the O plates, and 20 for the E plates.

(ii) The southern sky survey is based on 5.8×5.8 deg^2 scans of glass copies of the UKST B_J sky survey and originals of the current UKST SES and Equatorial R surveys. The UKST field centres are on a 5° grid and, unlike the old Palomar plates, have density wedges present in the SE and NW corners. The limiting magnitude is approximately 22.5 for the B_J plates and 21 for the R plates.

(iii) All plates were scanned using a 0.5-arcsec sampling interval and a scanning spot resolution of 1 arcsec. The image detection thresholds on the O and E plates were around 24 and 23 mag arcsec^{-2} respectively. For the B_J and R plates the equivalent numbers are 25 and 24 mag arcsec^{-2}.

(iv) Detected images were parametrized to preseve coordinate, intensity and general shape information and images on the comparison plate (B_J or O) were matched up with those on the reference plates (R, OR or E). The on-line APM catalogues, which form the raw data base for the carbon star survey, use a compressed subset of the parameters, namely x and y plate coordinate, magnitude, semi-major axis radius at detection isophote, ellipticity and ellipse position angle, image morphological classification and a 'stellarness' index.

(v) The instrumental magnitudes were initially internally mapped to a 'linear' magnitude scale using the technique described by Bunclark & Irwin (1983). These instrumental magnitudes were then transformed such that the derived photographic colours correctly described the known properties of the foreground Galactic stellar population (e.g. Demers et al. 1986). Finally, the Guide Star Photometric Catalogue (Lasker et al. 1988) which covers, albeit sparsely, most of the R magnitude range of interest was used to check, and if necessary update, the magnitude scale.

(vi) Over the magnitude range of interest $11 \lesssim R \lesssim 17$ and $14 \lesssim B \lesssim 20$, random magnitude errors are typically 0.1 mag, and the random errors in the colour index are typically 0.1–0.2 mag. Systematic field errors are also present at the ± 0.1 mag level and were mapped out of the colour domain using techniques similar to those described by Demers & Irwin (1987). Any systematic errors in the magnitude scale were ignored, since they are small relative to the uncertainties in converting R magnitudes into approximate distances.

(vii) Absolute astrometry was done using the relevant 200 + PPM astrometric standards per sky survey field (Roeser & Bastian 1988). These were used to define a linear coordinate transformation from machine x,y units to standard coordinates with respect to the plate centre ξ,η and thence to α,δ. Derived coordinates are typically accurate to 0.5 arcsec on both axes.

4.2 Candidate selection

Candidate cool carbon stars are selected using a colour–magnitude diagram (CMD) constructed from either UKST B_J, R survey plates, POSS2 B_J, R survey plates, or POSS1 O, E survey plates. To be included on the CMD, objects have to be classified as stellar on the reference red plate and have a matching image (any classification) present within 2 arcsec of the expected position on the blue comparison plate. An example of a high-latitude field CMD is given in Fig. 1. The positions of two AGB N-type carbon stars are shown superimposed. These passbands are particularly adept at selecting cool AGB carbon stars, because the colour at the tip of the giant branch $B_J - R \gtrsim 2.4$, equivalent to $B - V \gtrsim 1.9$, lies redward of most Galactic foreground contamination or any

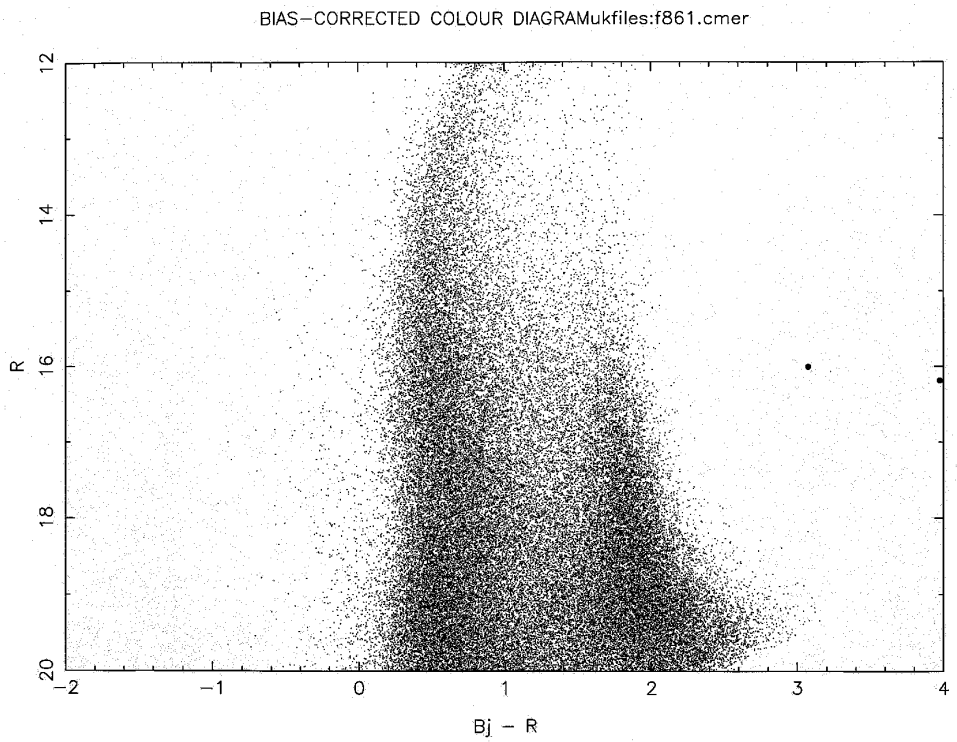

Figure 1. An example of a high-latitude B_J-R colour–magnitude diagram, illustrating the paucity of candidates redward of the survey limits: $B_J-R\gtrsim 2.4$ and $11\lesssim R\lesssim 17$. The filled circles denote the position of two N-type carbon stars found in this field.

other possible population, particularly for $R\lesssim 18$. The other obvious features of the CMD are the 'ridges' due to the varying mix of different Galactic foreground population components.

To facilitate comparison with other carbon star surveys, we give approximate linear relations between the various passbands used and the standard B and V passbands (Evans; Irwin, Demers & Kunkel 1990):

$$B_J-R=1.25(B-V),$$

$$O-E=1.8(B-V).$$

The colour differences between the three R bands used are small enough, ± 0.1 mag, to ignore (e.g. Evans 1988). These relationships are strictly only valid up to $B-V\approx 2$; therefore, as a check on internal consistency between B_J-R and $O-E$ selection, carbon stars in the $-3^\circ<\delta<3^\circ$ zone were used to directly map B_J-R on to $O-E$. A linear least-squares fit gives

$$B_J-R=0.67(O-E)+0.17,$$

which compares favourably, i.e. within ± 0.1 mag, with the previous equations over the range of interest. With a colour cut of $B_J-R\approx 2.4$, or $O-E\approx 3.3$, and a limit on R of $11\lesssim R\lesssim 17$, there are only a few candidates per field. The main contaminants are late-type M stars and K stars thrown into the sample because of photometric errors and plate flaws. APM finding charts of all the candidates are generated for both plates and visually inspected for obvious plate flaws and poorly measured images (e.g., objects within bright star haloes). Any remaining candidates are spectroscopically followed up.

The magnitudes of the previously known FHLC carbon stars lie in the range $11\lesssim R\lesssim 18$, with all but one having $R\lesssim 16.0$ (the exception is a very red carbon star at $R=17.0$ from the APM quasar survey). The bright survey limit of $R=11$, or roughly $V=12.5$, is equivalent to a Galactic z distance of ≈ 5–10 kpc, and is imposed to reduce the possibilty of contamination by thick disc or thin disc carbon stars. Also, for stars much brighter than this, the photometric errors start to rise appreciably due to the heavy saturation on the survey plates. For the APM quasar survey, which covered ≈ 2500 deg^2 of high-latitude sky, we systematically examined all extremely red objects to R magnitudes of $19+$, but found only one carbon star significantly fainter than $R\approx 16$. We are therefore restricting our 'all sky' survey to R magnitudes brighter than 17 to ensure that the number of candidates is kept to a minimum. Although dust-enshrouded carbon stars may appear fainter than this limit, it is unlikely that many 'normal' cool AGB carbon stars fainter than $R=17$ would be found anyway, since this would correspond to Galactic distances >100 kpc.

Our candidate selection followed the criteria described above. However, for the sake of completeness, and for the purpose of cross-checking carbon star properties, we have observed, and included in Tables 3 and 4, several previously known FHLC stars which may be brighter and/or bluer than the survey criteria.

4.3 Survey completeness

Apart from the relative insensitivity to the bluer CH-type carbon stars, there are three main reasons why the candidate selection will not be 100 per cent complete.

First, although image crowding is not a severe problem in high-latitude fields, up to 10 per cent of images can overlap other images at the detection isophotes used. For long-exposure UKST survey plates the typical FWHM of stellar images is between 2 and 3 arcsec. This causes a varying fraction of the images to overlap neighbouring images, making it difficult both to detect them as discrete entities and to estimate reliable magnitudes. In order to keep the number of candidates to a minimum, we required images to be classified by the APM as stellar on the R plate, and to be approximately stellar on the B_J plates (i.e., not obviously overlapped with neighbours, and clearly not background galaxies). This produces a much cleaner CMD with significantly fewer outliers at the expense of losing a few per cent of the real outliers. Secondly, the image classifier is statistical in nature and, at the magnitudes of interest, can misclassify up to 5 per cent of the images due to faint overlapping images, spurious grain noise, etc. Finally, photographic plates suffer both from systematic, or field, errors at the ± 10 per cent level and random photometric errors at the 5–10 per cent level. Of necessity this causes the colour selection, and to a lesser extent the magnitude boundary, to be somewhat 'fuzzy' with respect to true colours and magnitudes.

Taken together, these artefacts of selection from photographic survey material imply that we will miss between 10–20 per cent of the true outliers in a CMD, and they are consistent (albeit with small-number statistics) with the number of carbon stars found in common in the overlapping regions between different fields.

5 SPECTROSCOPIC OBSERVATIONS

We have now spectroscopically surveyed all of the SGC region above $\delta = -18°$, apart from a few fields still awaiting UKST R survey plates, and of the NGC fields above $\delta = -18°$, roughly half have been completed yielding a total of over 40 FHLC stars. The new observations were mainly taken over two one-week runs on the 2.5-m Isaac Newton Telescope, La Palma, in 1995 August and 1996 March using the IDS system. An additional series of service observations were also carried out on our behalf using the same set-up.

We observed candidates in two separate wavelength regions. To derive radial velocities we have taken $\sim$2.0-Å resolution spectra covering the wavelength region from 7500–8500 Å, which contains several CN carbon star absorption bands and a deep TiO absorption band for M stars. This enabled us to verify the candidate type for new objects and simultaneously to obtain a radial velocity for the carbon stars. These observations were taken using the Tek3 CCD, the R831R grating and the 235-mm camera, giving an effective wavelength coverage of $\approx$1200 Å and a resolution of $\sim$2.4 Å (1.2 Å per pixel). This corresponds to a velocity resolution of 45 km s^{-1} per pixel or $\sim$90 km s^{-1} per resolution element.

In addition, we have obtained low-resolution spectrophotometry of all the carbon stars in the wavelength region 4000–7500 Å. These observations were taken with the Tek3 CCD, the R300V grating and the 235-mm camera, giving an effective wavelength coverage of 3500 Å and a resolution of 3.0 Å per pixel. In this wavelength region CH-type carbon stars have a well-defined absorption feature at 4300 Å due to the G-band of CH, enabling us to readily distinguish between CH- and N-type carbon stars while simultaneously acquiring low-resolution spectrophotometry for each carbon star.

For all observations the slit was oriented at the parallactic angle to minimize slit losses as a function of wavelength. For the high-resolution spectra the slit width was set to be 1.5 arcsec, which corresponds to 2 pixels on the detector – the resolution of the spectrograph. For the lower resolution spectrophotometry, slit widths ranging between 1.5 and 5 arcsec were used to help calibrate out slit losses. After each observation of a *new* carbon star, an arc lamp exposure was taken for accurate wavelength calibration. Suitable flux standards, atmospheric absorption standards and carbon stars of known radial velocity were observed regularly throughout each night of observation.

6 DATA REDUCTION

The data were reduced using the standard IRAF[3] software packages. A summary of the reduction steps for the spectra is provided below. As described in the previous section, we have taken observations in two separate wavelength regions. Higher dispersion spectra (7500–8600 Å) were taken to derive radial velocities in addition to extending the fluxed spectral range, and lower dispersion spectra (4000–7500 Å) were used to determine carbon star type and blue-end flux spectral coverage. Each spectrum, irrespective of the wavelength range observed, is initially processed in an identical manner.

6.1 Initial reductions and wavelength calibration

Each CCD image was debiased, trimmed and flat-fielded using 'CCDPROC'. Spectral extraction was performed by APALL, and the sky background was estimated by interpolating between specified background regions on either side of the object spectrum.

Combined CuNe + CuAr arcs were taken at regular intervals throughout the observations to provide accurate wavelength calibration, and were specifically taken after each observation of a carbon star, newly discovered or otherwise. The extraction of the arcs was carried out with the APALL routine using the preceeding star as an aperture reference, with profile fitting, background subtraction and cosmic ray cleaning disabled. Arc emission lines were identified from standard calibration maps and a pixel-to-wavelength calibration curve found by fitting a third-order Chebyshev polynomial to the calibration points using the IDENTIFY routine. Typical rms residuals from these fits for the high-resolution spectra were found to be 0.03 Å. The dispersion solution was applied to the extracted spectra, which were then put on a linear wavelength scale using DISPCOR. The sky emission lines, which had also been extracted concurrently with object spectra, were wavelength-calibrated in the same manner, and were then cross-correlated with each other using FXCOR to verify the accuracy of the wavelength calibrations. Pixel shifts < 0.1 pixel were found, corresponding to velocity shifts of < 3 km

[3]IRAF is distributed by the National Optical Astronomy Observatories.

s^{-1}, suggesting that induced errors caused by spectrograph flexure and/or wavelength calibration are negligible compared to the desired target accuracy of 5–10 km s^{-1}.

6.2 Carbon star selection

A quick-look spectral extraction was performed in pseudo-real time at the telecope to pick out obvious carbon stars for further study. From the point of view of spectral classification these quick-look spectra are comparable to the examples of the final extracted spetra shown in Fig. 2, where we show the spectra of an N-type carbon star together with late dwarf stars of M and K types. Clearly, carbon star spectra are readily distinguishable from contaminant M- and K-type stars. In the wavelength region 7800–8400 Å, carbon star spectra contain several CN absorption bands, whilst M-type stars show deep TiO and VO absorption bands.

6.3 Atmospheric absorption correction

To correct for atmospheric absorption, a spectrum which contained only sky absorption lines was required. Taking the observed absorption standard spectrum, we used SPLOT and the XX command to 'snip' out the absorption lines and the resultant image was saved. Dividing the original absorp-

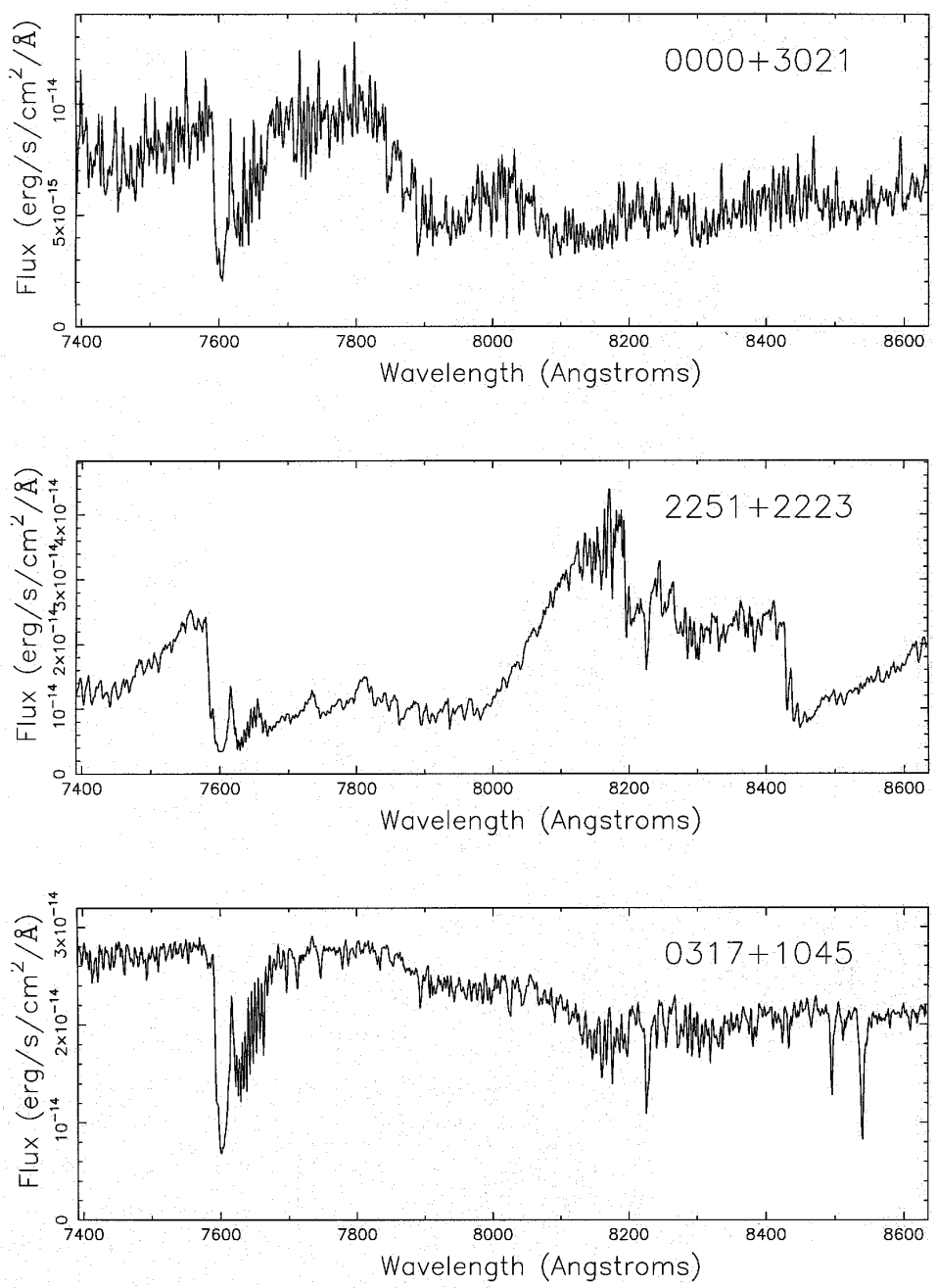

Figure 2. Spectra of an N-type C star, an M-type star and a K-type star in the wavelength range used for the survey phase. FLHC stars are clearly discernible from M- and K-type contaminants in the candidate sample.

tion spectrum by the new image then gave a spectrum which had a continuum of 1.0 containing only the sky absorption lines. This correction spectrum is then suitably scaled and used to normalize out atmospheric absorption features in the target object spectra. Slight adjustments to the scaling factor are often needed because of localized changes in the atmosphere throughout the night. For any night which had no absorption standards observed, the nearest standard was used, with special care being taken with the scaling factor needed for complete absorption correction.

This method of absorption correction is quite effective; however, it must be stressed that the correction used for each spectrum is heavily dependent on the scaling factor used. Also, the point of complete correction is often a subjective decision on the part of the person reducing the data. Atmospheric absorption corrections were carried out only for the high-resolution spectra, i.e., for the wavelength region 7500–8600 Å. There were no significant absorption effects in the low-resolution data.

7 RADIAL VELOCITIES

A selection of carbon star radial velocity 'standards' were observed at regular intervals throughout each night (see Table 2). Standard radial velocity stars were chosen from the Bright Star Catalogue. We selected carbon stars of spectral type as close as possible to the programme objects, although in practice the limited number of available carbon star velocity standards led to some spread in their spectral type relative to the programme objects. Cross-checks between the different standard stars and the programme objects indicated that any systematic effect induced by spectral mismatch was well below 10 km s^{-1}. We suspect that the relative insensitivity to spectral type in the near-infrared part of the spectrum is due to the well-defined cross-correlation peaks arising from the many narrow CN absorption lines superimposed on a smoothly varying continuum. By rectifying the spectra before cross-correlation, global continuum changes caused by varying spectral type are effectively removed, whilst all the carbon stars studied have well-defined CN lines. These standards were processed using a method identical to that used for the FHLC star candidates. Radial velocities were computed via Fourier cross-correlation using the FXCOR routine in IRAF. The following procedure was repeated using each radial velocity standard as the template spectrum.

The spectra must be initially prepared for cross-correlation. Since we have by default used a linear wavelength scale, the spectra were rebinned to a logarithmic scale where the rebinning was defined by the spectra of smallest dispersion. The spectra are then interactively continuum-subtracted. We tried various degrees of rectification and found that there was no significant change ($\sim$0.1 km s^{-1}) in the radial velocity computed when using either a cubic spline of order 1 (basic rectification) or a cubic spline of order 20 (complete rectification). All the spectra were therefore continuum-subtracted using a cubic spline of order 1.

Apodization at the end of the spectra was set to zero per cent, as this was found to have little effect on the radial velocity calculations since the rectified continua were already close to zero at the ends. The complete high-resolution spectrum was used for the cross-correlation to allow as much spectral information as possible to be extracted from each spectrum. Tests were made to assess the effect of possible residual telluric lines by excising the main atmospheric absorption bands and repeating the cross-correlation. In all cases no significant change was noted. The peak of each cross-correlation function is then interactively fit with a Gaussian function to derive an accurate estimate of the shift between the template radial velocity standard and the object spectrum.

Using VHELIO from the template spectra header and UT and EPOCH from the header of the image spectra, FXCOR then calculates the topocentric and heliocentric corrections for the object spectra, outputting the relative velocity shift, the observed velocity for the object, and the heliocentric velocity for the object.

For each carbon star observation we therefore have a heliocentric velocity for each template radial velocity standard with which it is cross-correlated. Several carbon stars were observed on more than one night, and so their average heliocentric velocities are quoted.

Table 2. Radial velocity standards.

Standard	No. of Observations	v_{pub}	v_r (km/s)	σ
2142+3530	5	+10	+7	5
HR2308	1	+12	+7	
0849+1736	2	−1	−1	12
1240+4559	3	+12	+28	5
HD16115	3	+14	+4	1

Notes:
v_{pub} is the published value for the radial velocity for each star.
v_r is the average radial velocity deduced from cross-correlation with the other templates.
σ is the standard error in velocities calculated from repeated observations.

7.1 Errors in the radial velocities

Velocity errors that affect the final results include wavelength calibration problems associated with spectrograph flexure, offsets caused by not centring an object correctly in the slit, mismatched template versus programme stars leading to velocity shifts, and random errors due to signal-to-noise ratio limitations, mainly from the much fainter programme stars. Programme stars have typical integration times ranging from 300 to 900 s, leading to continuum signal-to-noise values of $\gtrsim$10 per pixel. At this signal-to-noise level the near-infrared CN bands in carbon stars are well defined and lead to good-quality cross-correlation peaks (e.g. Fig. 3). With this quality of spectra the random rms error from fitting the cross-correlation peak is roughly 1–2/10ths of a pixel, or 3–7 km s^{-1}. Shifts due to wavelength calibration errors and/or flexure of the spectrograph were estimated to be <3 km s^{-1} by examining the repeatability of the positions of the sky lines, as outlined earlier. Template-

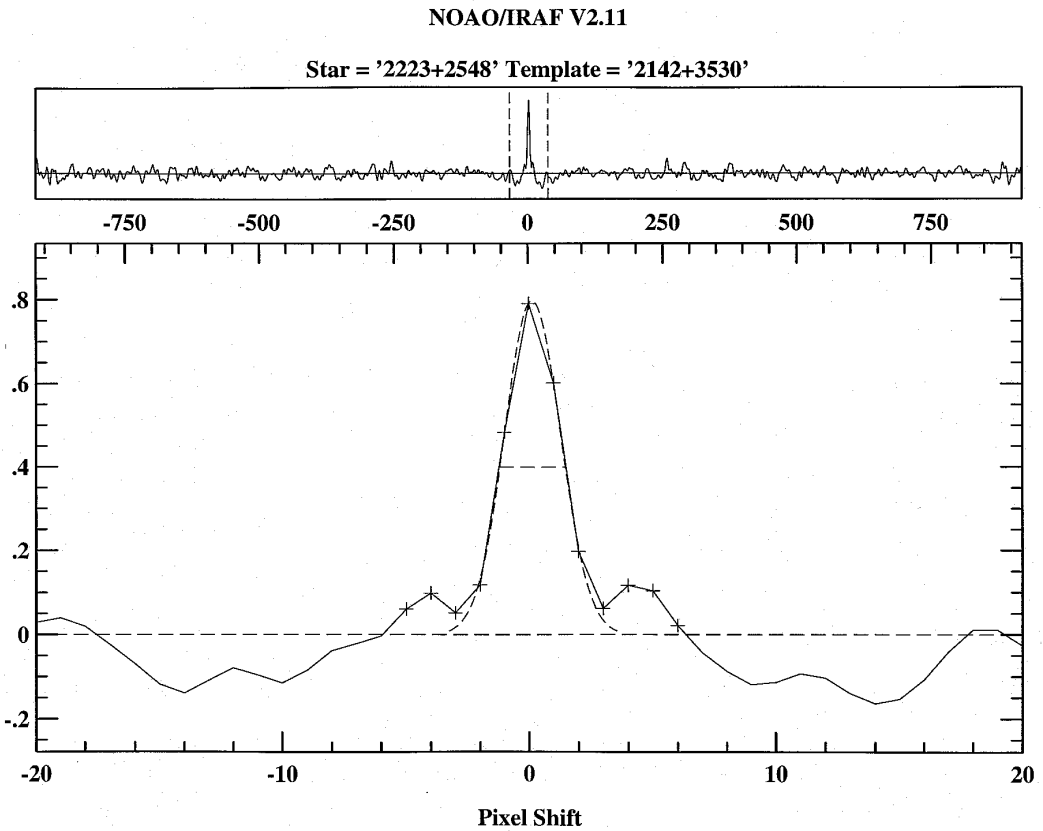

Figure 3. An example of the cross-correlation carried out for each carbon star in order to determine precise radial velocities.

induced errors and slit centring problems are investigated below by analysing the internal consistency and repeatability of the standard star derived velocities.

Table 2 lists the radial velocity (RV) standards used throughout our observations. Most of the RV standards were observed more than once, and in total we effectively have 14 radial velocity standard observations. Each RV standard observation was cross-correlated against the other RV standards as a further check on possible velocity errors. Column 4 in Table 2 lists the estimated mean radial velocity of each standard derived from cross-correlating against the other standard star templates. These velocities can be compared with the published radial velocities as a check on both the reliability of the published velocity of a particular standard and the validity of using it as a standard template. Repeat measurements of the same radial velocity standard are mainly useful in assessing the effects of slit centring errors, since the accuracy of the wavelength calibration (<3 km s^{-1}) has been independently checked for all observations using the sky lines. The standard error, σ, due to repeated observations of the same standard star can be derived from

$$\sigma^2=\frac{1}{n-1}\sum_{i=1}^{n}(x_i-\langle x\rangle)^2, \qquad (1)$$

where n is the number of repeat observations, and $\langle x\rangle$ is the average of the n observations. In this case each individual velocity is, as before, the average of the cross-correlation with respect to all the other standard stars. The typical variation from repeat observations of the same standard is of order 5 km s^{-1}. Most of this variation is likely to be caused by slit centring errors, and we take this value as an indicator of the likely size of this effect, although we note that for longer integrations on target objects the slit centring error is likely to be smaller than this.

It can be seen from Table 2 that the radial velocity standards $1240+4559$ and HD 16115 have average velocities which differ significantly from their published values. It is now well known that a significant fraction of AGB carbon stars are atmospheric velocity variables with typical velocity changes up to 10 km s^{-1} or more. Examples of this effect for a similar sample of cool AGB carbon stars found in the haloes of the Magellanic Clouds are presented by Kunkel et al. (1996). It is possible that some of the standards may have variable radial velocities, or that some of this variation is caused by template mismatch between the different standards (which cover the spectral range of the programme stars). However, since the total spread in velocities found for these standard stars is only of order ± 5 km s^{-1} we have simply taken the average of the fits of all templates to the programme stars to define our velocity system zero-point.

The combined effect of all the errors means that the majority of the programme stars have a velocity precision between 5 and 10 km s^{-1}. Since this range is at the lower end of the velocity dispersion found in dwarf satellite galaxies, it is more than adequate to investigate possible tidal systems.

8 FLUX CALIBRATION

Several bright flux standards were observed each night. The packages within IRAF which are used to carry out the flux calibration require that the exposure time and airmass be included in the image header. This required editing the image headers to include the fields 'EXPTIME' and 'AIRMASS'. The package STANDARD was used to add the standard stars to the sensitivity file. The spectra of the observed standard stars are integrated over the calibration bins and, along with the associated calibration fluxes from tabulated calibration data, are used by the routine SENSFUNC to determine the system sensitivity as a function of wavelength for the aperture used. The raw sensitivity functions were then 'filtered' by fitting an order-3 cubic spline to derive the final smooth sensitivity function. The typical rms error on the fits was at the level 2 per cent.

The object spectra are then corrected for extinction, and calibrated to a flux scale using the sensitivity function produced by SENSFUNC. We have used f_λ as the flux scale in all the figures to help to emphasize the rather faint blue end of the spectra. The high- and low-resolution spectra – where available – were combined using the overlap region to produce a single fluxed spectrum (see Fig. 5). For those objects without low-resolution spectra we show the high-resolution red end only, in Fig. 6.

As a further check against slit losses, each low-resolution spectrum was scaled such that integrating over the R passband gave an R magnitude equivalent to those measured from the APM scans for that star.

9 SURVEY RESULTS

We have now surveyed all of the SGC region accessible from La Palma to within 30° of the Galactic plane (apart from an area bounded by a few UKST fields without survey R plates) and some of the NGC region. We are aiming to finish off the survey in two phases: first by completing the search in the NGC region using a mixture of UKST and POSS1/POSS2 sky survey plates, and secondly by extending the survey south of $\delta = -20°$ using UKST survey plates. The southern part of the SGC is particularly interesting, since this is where the majority of gas in the Magellanic Stream is to be found. So far we have surveyed a total of ~ 7000 deg^2 of high-latitude sky and found 41 carbon stars that satisfy the survey criteria. We estimate our survey completeness for cool carbon stars to be ≈ 80 per cent (see Section 4.3 for more details), implying a surface density of faint N-type carbon stars at high galactic latitudes of 1 per ≈ 200 deg^2.

Tables 3 and 4 summarize the results of the APM Carbon Star Survey. A few of the objects listed are included because of their intrinsic interest and to help tie in with other survey work. The velocity errors quoted in Table 4 are solely those derived from the fit to the cross-correlation peak, and do not include the systematic errors of 5–10 km s^{-1} from other sources discussed earlier. If we combine the systematic and random errors in quadrature, then the overall velocity error for most objects in Table 4 is close to ± 10 km s^{-1}. Several of the APM-selected carbon stars had already been classified as carbon stars from previous work. From the total number of APM-selected carbon stars, between six and nine of the carbon stars are CH-type carbon stars; the remainder are N-type carbon stars with a few apparently reddened by dust and a few others showing emission lines. APM-generated finding charts for the carbon stars listed in Table 3 are shown in Fig. 7.

9.1 Comparison with other surveys

It can be seen from Table 3 that we have 'rediscovered' all of the previously published faint N-type carbon stars in the Galactic halo. Our derived radial velocities for these stars in Table 4 can be compared with the previously published values in Margon et al. (1984), Mould et al. (1985), Nguyen-Q-Rieu et al. (1987) and Bothun et al. (1991). The N-type carbon star $1509-0902$, observed by Margon et al., had a derived radial velocity of 75 ± 40 km s^{-1}, agreeing well within the errors. The very red star, $1523+4235$, discovered by Sanduleak & Pesch (1982), has two radial velocities quoted by Mould et al., -72 ± 1 and -62 ± 4 km s^{-1}, both

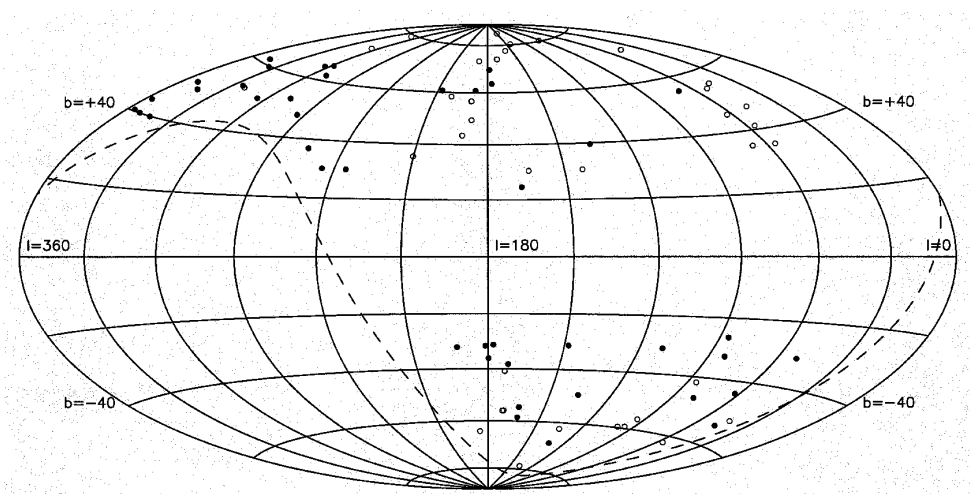

Figure 4. The spatial distribution of all the currently known high-latitude distant carbon stars, shown in an Aitoff projection. Filled circles denote carbon stars satisfying the APM survey criteria. The dashed line denotes the limit $\delta = -18°$.

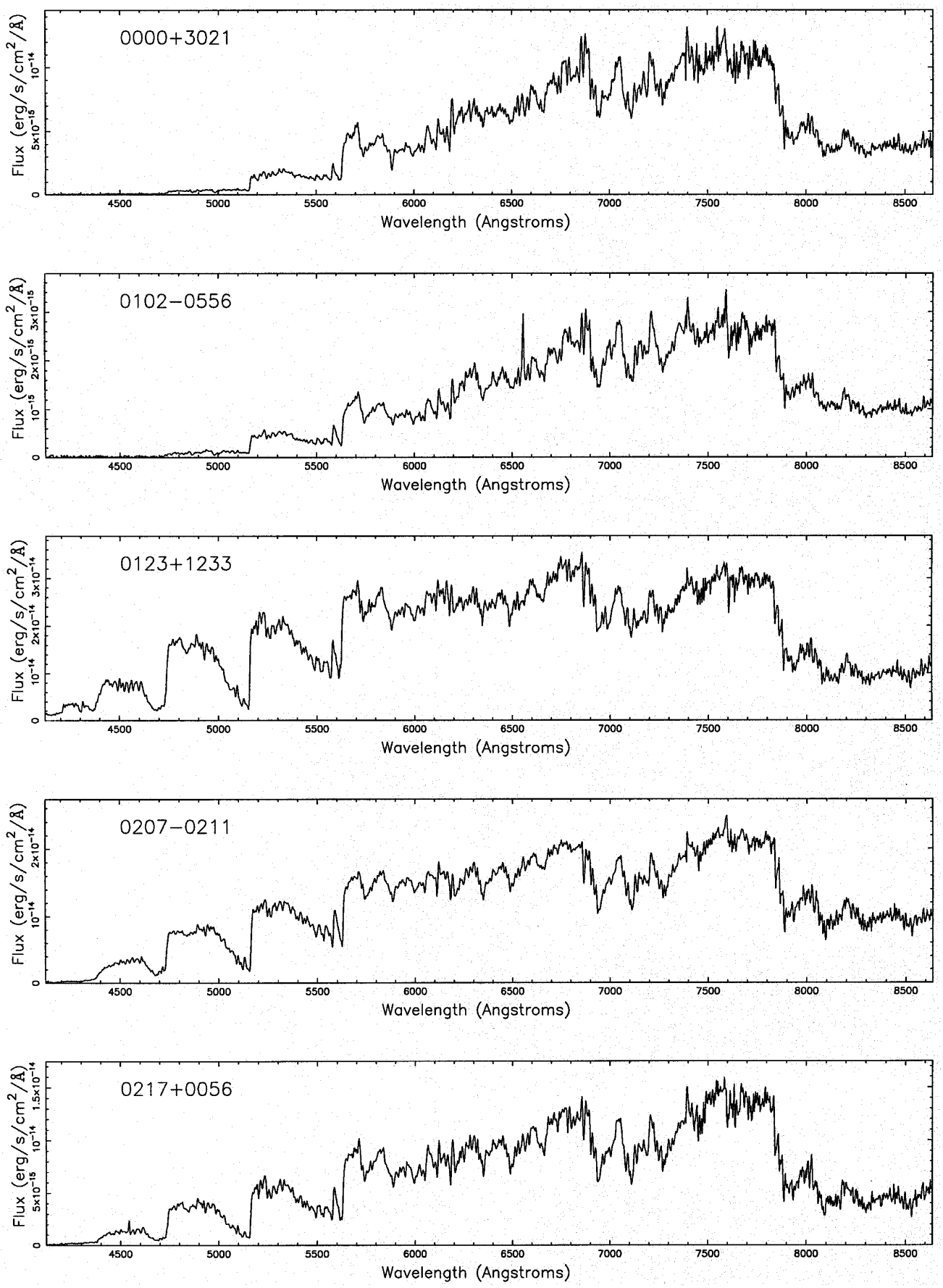

Figure 5. Spectra for APM carbon star survey.

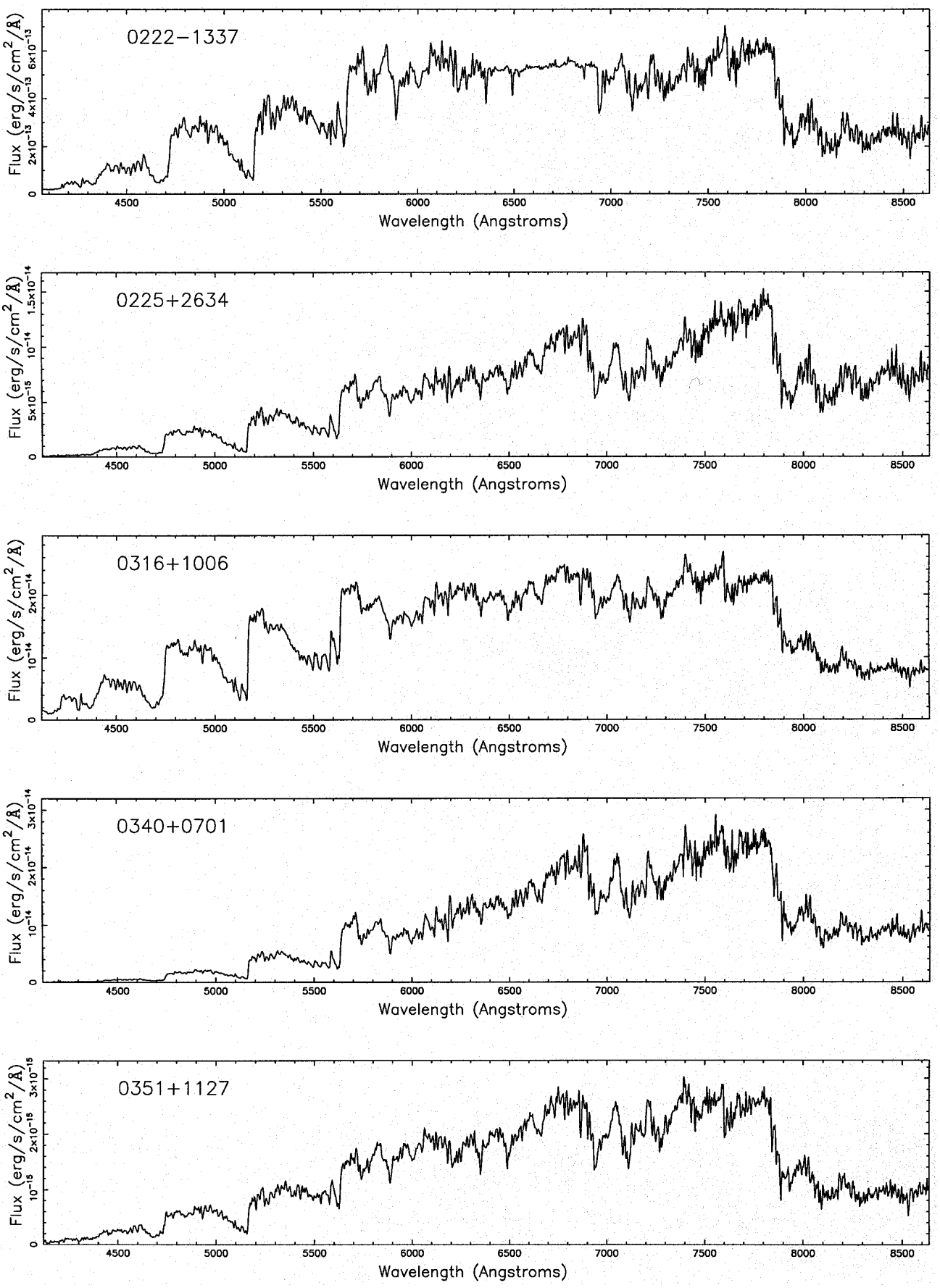

Figure 5 – *continued*

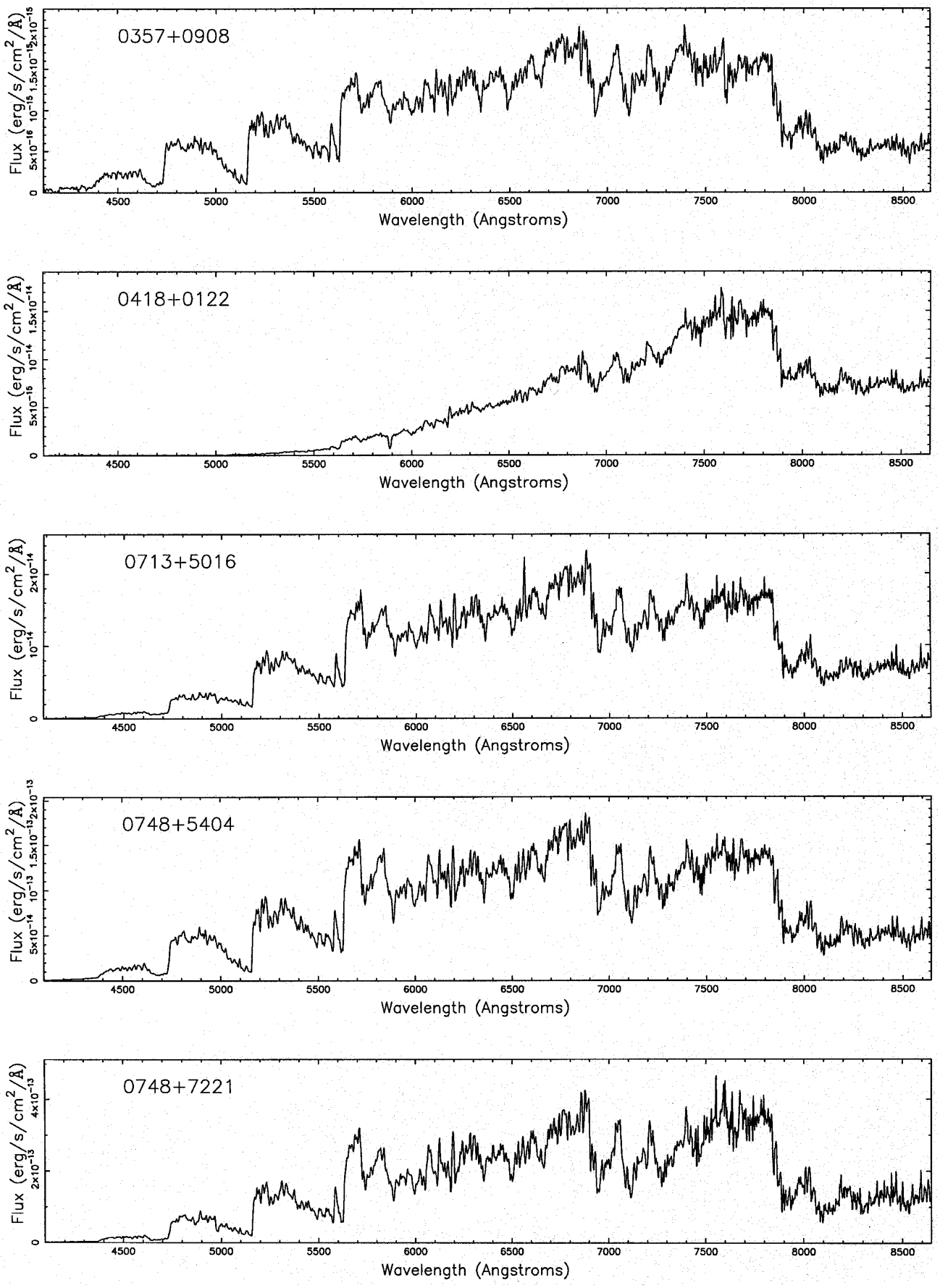

Figure 5 – *continued*

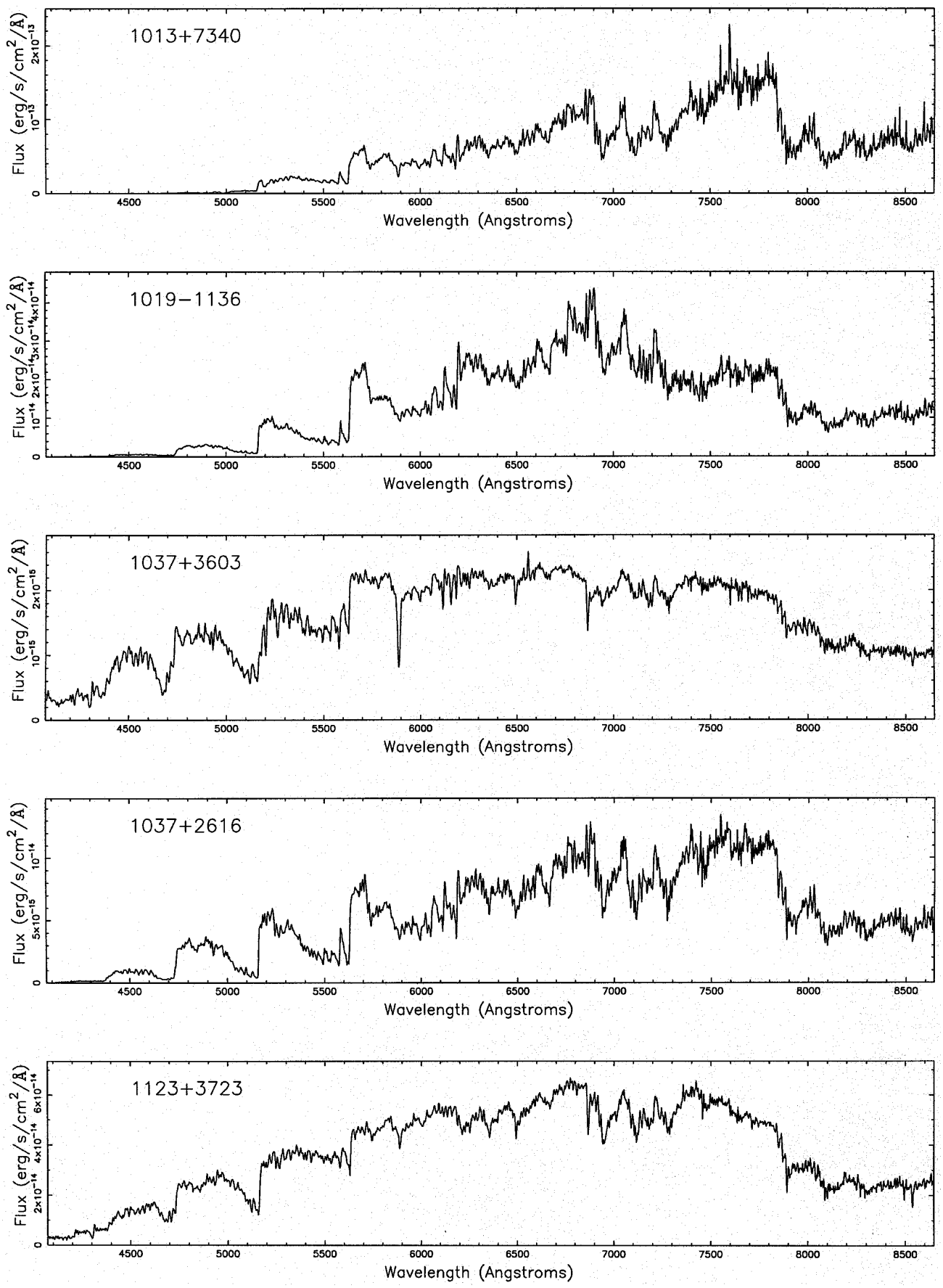

Figure 5 – *continued*

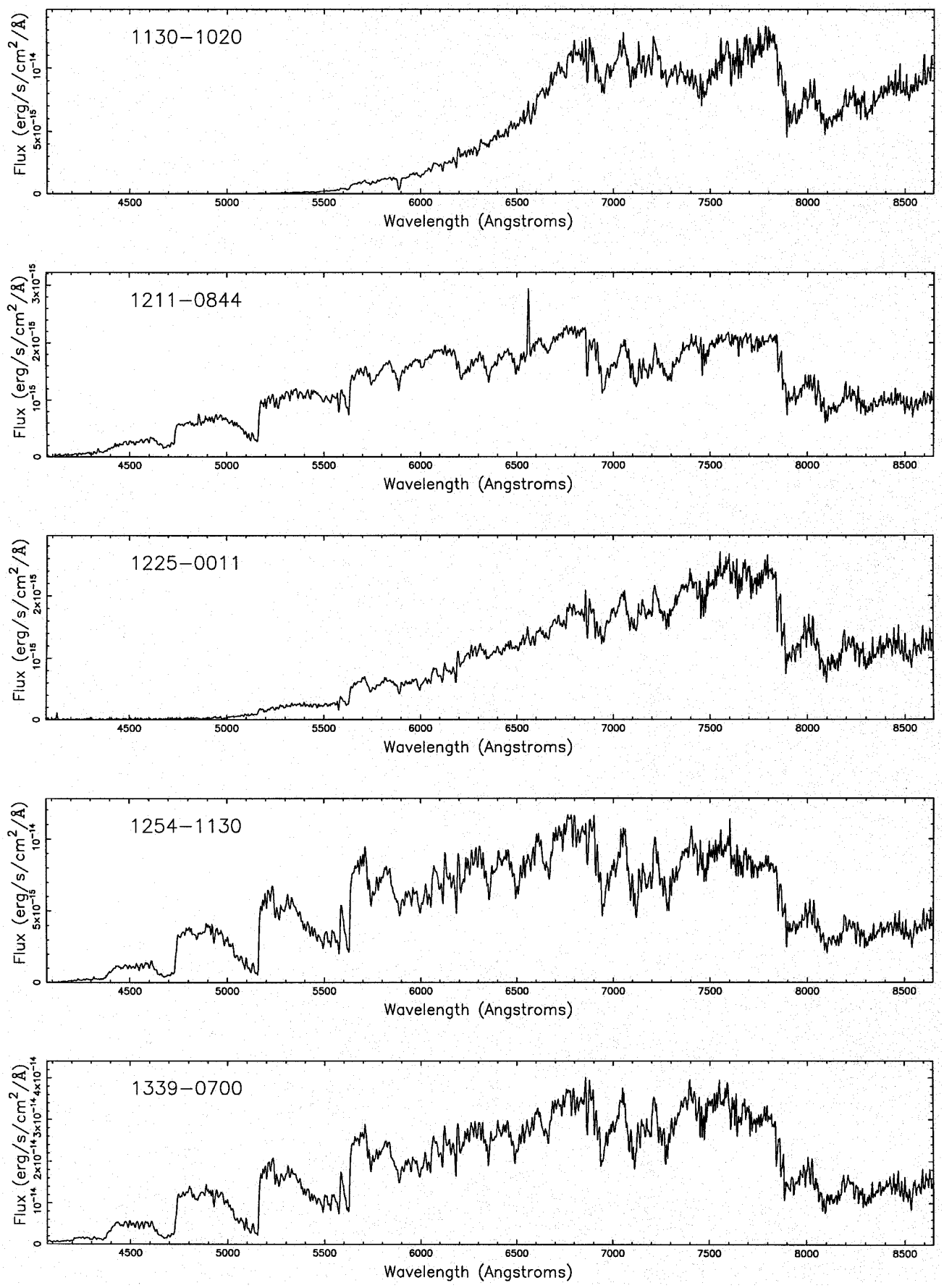

Figure 5 – *continued*

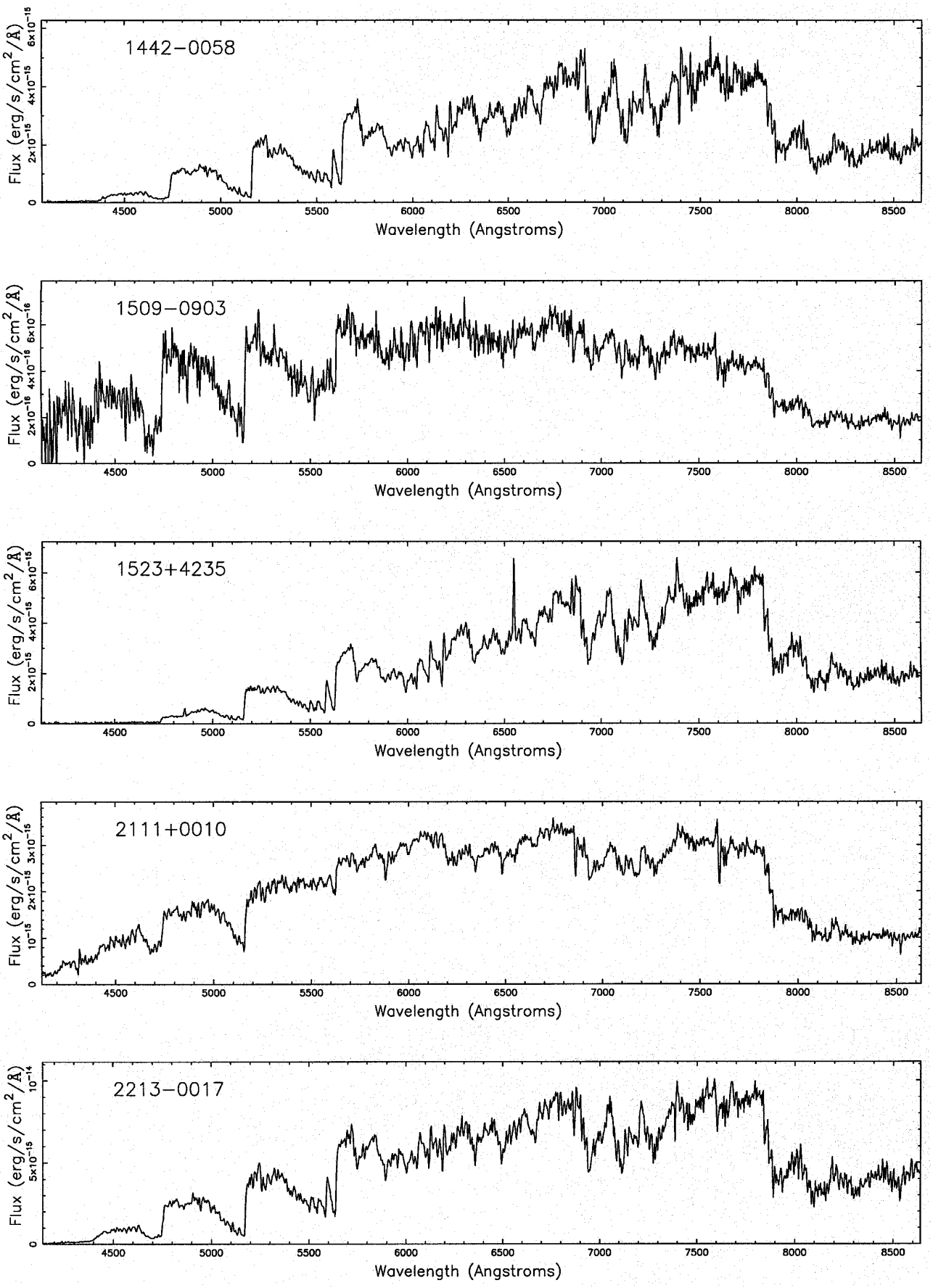

Figure 5 – *continued*

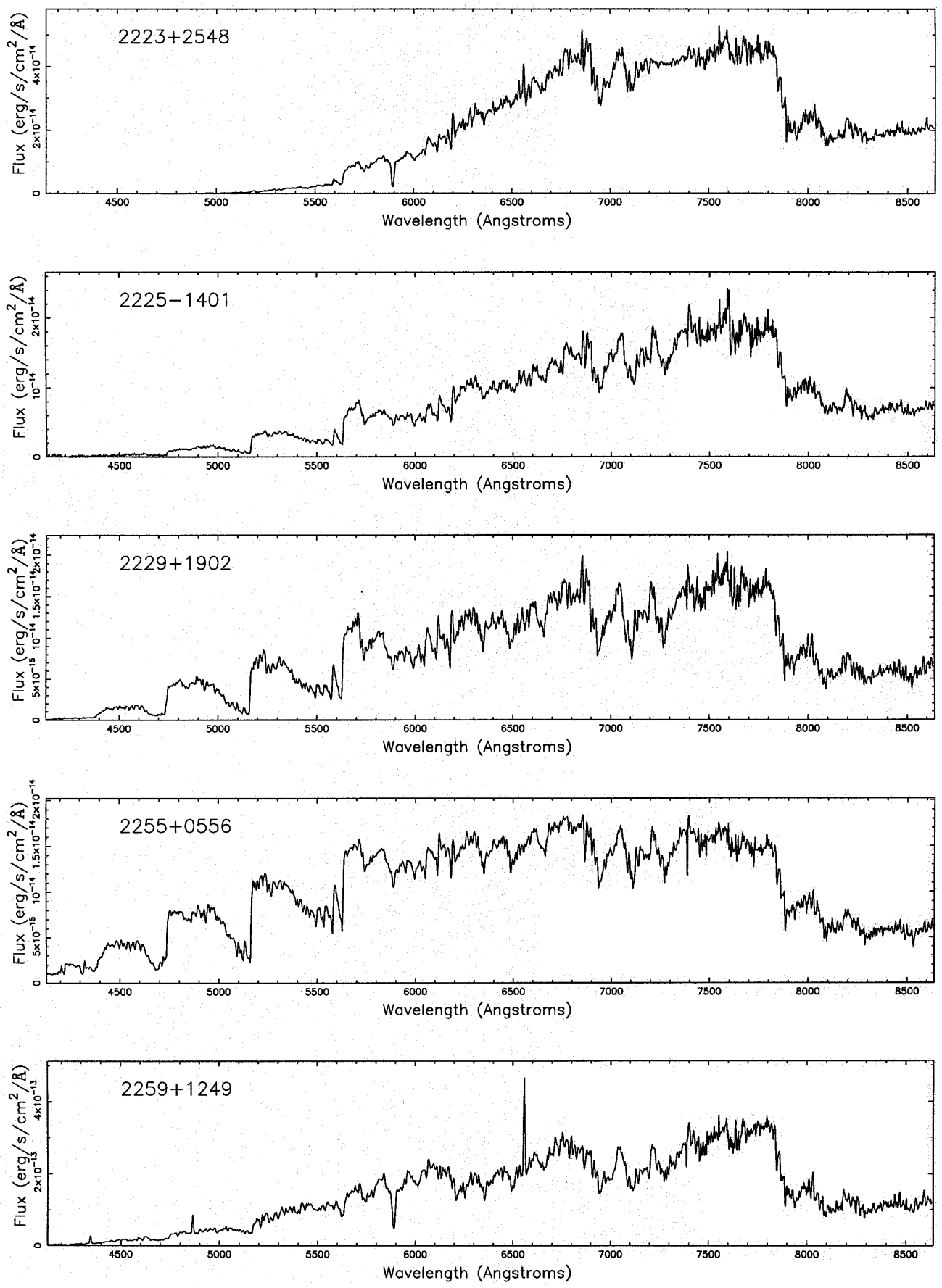

Figure 5 – *continued*

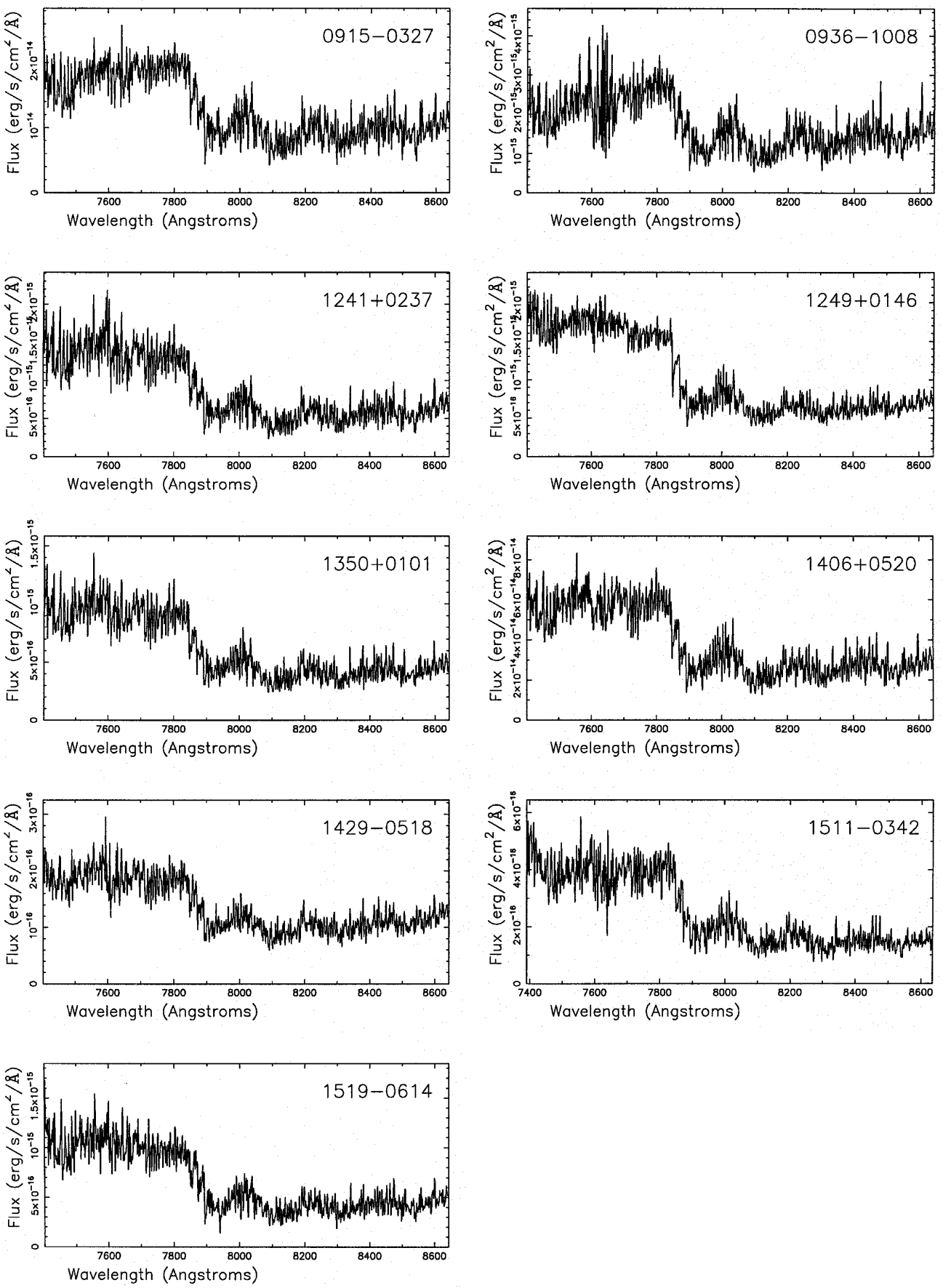

Figure 6. Spectra of carbon stars with no blue-end observations.

Table 3. High-latitude distant cool carbon stars – magnitudes and spectral types.

Ra	Dec	R	$B_J - R$		Comments
00 00 26.8	+30 21 41	13.8	3.2	APM	N-type
01 02 28.2	−05 56 08	15.3	2.8	C*07 + APM	N-type + em lines
01 23 34.6	+12 33 05	12.3	2.4	Stephenson + APM	CH-type
02 07 39.6	−02 11 47	12.8	4.9	C*30 + APM	N-type
02 17 49.0	+00 56 57	13.4	2.9	C*31 + APM	N-type
02 22 44.2	−13 37 31	9.0	2.0:	C*15	CH-type
02 25 53.1	+26 34 19	13.6	3.1	APM	N-type
03 16 08.3	+10 06 08	12.6	2.3	APM	CH-type
03 40 48.2	+07 01 31	13.0	3.5	APM	N-type
03 51 30.9	+11 27 32	15.1	2.5	APM	CH/N-type
03 57 30.2	+09 08 43	15.5	2.8	APM	N-type
04 18 51.9	+01 22 11	14.0	6.6	APM	N-type + dust
07 13 46.6	+50 16 05	12.9	3.6	APM	N-type + em lines
07 48 08.6	+54 04 40	10.6	2.3	Stephenson	N-type
07 48 34.2	+72 21 33	9.9	2.5	Stephenson	N-type
09 11 48.7	+33 41 29	12.9	1.2	CLS9	CH-type
09 15 37.2	−03 27 18	12.2	2.7	APM	CH-type
09 36 33.7	−10 08 11	15.9	2.6	APM	N-type:
09 39 45.9	+36 30 45	14.5	1.1	CLS14	CH-type
10 13 37.9	+73 40 12	11.3	4.3	Stephenson + APM	N-type + dust?
10 19 46.8	−11 36 28	12.5	3.0	APM	N-type
10 37 15.7	+36 03 44	14.3	2.1	CLS29 + APM	CH-type + em lines
10 37 18.3	+26 16 53	13.7	2.8	APM	N-type
10 56 35.2	+40 00 12	12.3	3.3	FBS + APM	N-type:
11 23 34.4	+37 23 58	11.5	2.4	CLS38 + APM	CH-type
11 30 52.3	−10 20 24	14.0	9.1	IRAS1130-1020 + APM	N-type + dust
12 11 42.6	−08 44 11	15.2	3.3	APM	N-type + em lines
12 25 06.2	−00 11 16	15.7	3.2	APM	N-type + dust
12 41 04.1	+02 37 56	16.0	3.1	UM515 + APM	N-type:
12 49 16.5	+01 46 18	15.8	4.0	APM	N-type:
12 54 20.0	−11 30 06	13.6	2.8	APM	N-type
13 39 49.5	−07 00 17	12.3	2.6	APM	CH/N-type
13 50 28.0	+01 01 59	15.9	3.8	APM	N-type:
14 06 04.5	+05 20 38	12.0	3.4	Stephenson + APM	N-type:
14 29 51.1	−05 18 06	17.0	>4.5	APM	N-type: + dust
14 42 14.3	−00 58 18	14.6	3.4	APM	N-type
14 50 58.9	−13 00 53	15.2	3.8	APM	N-type:
15 09 46.7	−09 02 50	16.5	2.0	Margon *et al.*	CH-type
15 11 04.5	−03 42 39	15.2	3.0	APM	N-type:
15 19 57.1	−06 14 55	15.3	3.5	APM	N-type:
15 23 53.3	+42 35 18	14.5	4.8	Sanduleak & Pesce+APM	N-type+emlines
21 11 26.6	+00 10 34	14.7	2.6	APM	CH-type
22 13 03.2	−00 17 57	13.8	3.2	APM	N-type
22 23 58.6	+25 48 20	12.3	5.5	Stephenson + APM	N-type + dust + em lines
22 25 30.3	−14 01 44	13.4	3.4	APM	N-type
22 29 28.0	+19 02 14	13.2	2.6	APM	N-type
22 55 53.2	+05 56 20	12.9	2.4	APM	CH-type
22 59 16.9	+12 49 07	10.1	3.4	Stephenson	N-type + em lines

Notes:
Carbon stars labelled '+APM' are previously known stars satisfying our survey criteria; those labelled 'APM' are the newly discovered carbon stars; in addition, a few extra faint CLS carbon stars and other well-known carbon stars were observed for cross-calibration checks. Spectra for some of the carbon stars are shown in Fig. 5. For the remainder we do not yet have good-quality 'blue' spectra. Those carbon stars without available good quality 'blue' spectra, denoted by ':', have been assigned carbon types using the optical colours. As a general rule we find that carbon stars in the table with $B_J - R \gtrsim 2.5$ are N-type, and if $B_J - R \lesssim 2.5$ they are CH-type. Not all of the sky at high latitude has yet been surveyed, particularly for $\delta < -18°$. All coordinates are B1950. UM 515 was discovered in the University of Michigan Thin Prism survey but has not ben previously published. Stars labelled Stephenson are listed in the Catalogue of Cool Galactic Carbon Stars (Stephenson 1989).

Table 4. High-latitude distant cool carbon stars – radial velocities and distance estimates.

Star	$V_\odot$ (km/s)	V_{gal} (km/s)	Helio. dist. (kpc)	Galc. dist (kpc)	Previous $V_\odot$ (km/s)	Comments
0000+3021	−111 ± 3	67	29	32		
0102−0556	−74 ± 4	−20	58	60	21 ± 19 [3]	
0123+1233	−302 ± 7	−208	15	20		
0207−0211	−140 ± 5	−119	18	24	−131 ± 19 [3]	
0217+0056	−142 ± 3	−113	24	30	−138 ± 19 [3]	
0222−1337	−27 ± 4	−51	3	10	−11 ± 19 [3]	
0225+2634	−44 ± 5	50	26	33		
0316+1006	103 ± 4	124	17	24		
0340+0701	36 ± 3	20	20	27		
0351+1127	−132 ± 3	−138	53	60		
0357+0908	−141 ± 3	−158	63	71		
0418+0122	33 ± 4	−21	<32	<39		very red + dust
0713+5016	−3 ± 4	33	19	27		
0748+5404	0 ± 3	47	7	15		
0748+7221	−94 ± 4	21	5	12		
0911+3341	−7 ± 9	−47	19	26	−59 ± 19 [3]	
0915−0327	79 ± 4	−88	14	20		
0936−1008	260 ± 3	76	76	79		
0939+3630	139 ±21	122	40	46	123 ± 19 [3]	
1013+7340	−52 ± 5	64	<9	<16		+ dust ?
1019−1136	126 ± 4	−52	16	20		
1037+3603	−3 ± 6	−26	36	41	23 ± 4 [2]	
1037+2616	−98 ± 4	−152	28	32		
1056+4000			15	20		
1123+3723	29 ± 5	29	10	15	−24 ± 19 [3]	
1130−1020	36 ± 3	−116	<32	<32	24 ± 2 [4]	very red + dust
1211−0844	128 ± 3	2	55	54		
1225−0011	−35 ± 4	−133	<69	<68		+ dust
1241+0237	49 ± 4	−32	79	78		
1249+0146	51 ± 6	−27	72	71		
1254−1130	67 ± 4	−45	26	25		
1339−0700	−150 ± 4	−226	15	13		
1350+0101	39 ± 4	−6	76	72		
1406+0520	−21 ± 5	−37	13	11		
1429−0518	72 ± 5	41	<126	<121		very red + dust
1442−0058	37 ± 4	24	43	37		
1450−1300			55	49		
1509−0902	90 ±10	75	100	94	75 ± 40 [1]	
1511−0342	57 ± 4	64	55	49		
1519−0614	105 ± 4	106	58	51		
1523+4235	−67 ± 4	63	40	39	−72 ± 1 [2]	
2111+0010	−208 ± 7	−57	44	40		
2213−0017	−44 ± 3	98	29	27		
2223+2548	21 ± 7	223	<15	<16		very red + dust
2225−1401	−113 ± 5	−18	24	22		
2229+1902	−348 ± 3	−162	22	23		
2255+0556	−189 ± 4	−44	19	20		
2259+1249	17 ± 3	182	5	10		

Notes:
Distances are approximate and assume an average $M_R = -3.5$ for cool carbon stars; CH-types are likely to be somewhat fainter intrinsically than N-types and hence closer than estimated in the above table.
Objects without radial velocity entries have no suitable high-resolution spectroscopy available.
Stars with upper limits to the distances are likely to be significantly closer due to intrinsic dust extinction.
V_{gal} was computed assuming a solar motion of (9, 232, 7) km s^{-1} with respect to the Galactic Centre.
Previous work on velocities by [1]Margon et al. (1984), [2]Mould et al. (1985), [3]Bothun et al. (1991) and [4]Nguyen-Q-Rieu et al. (1987).

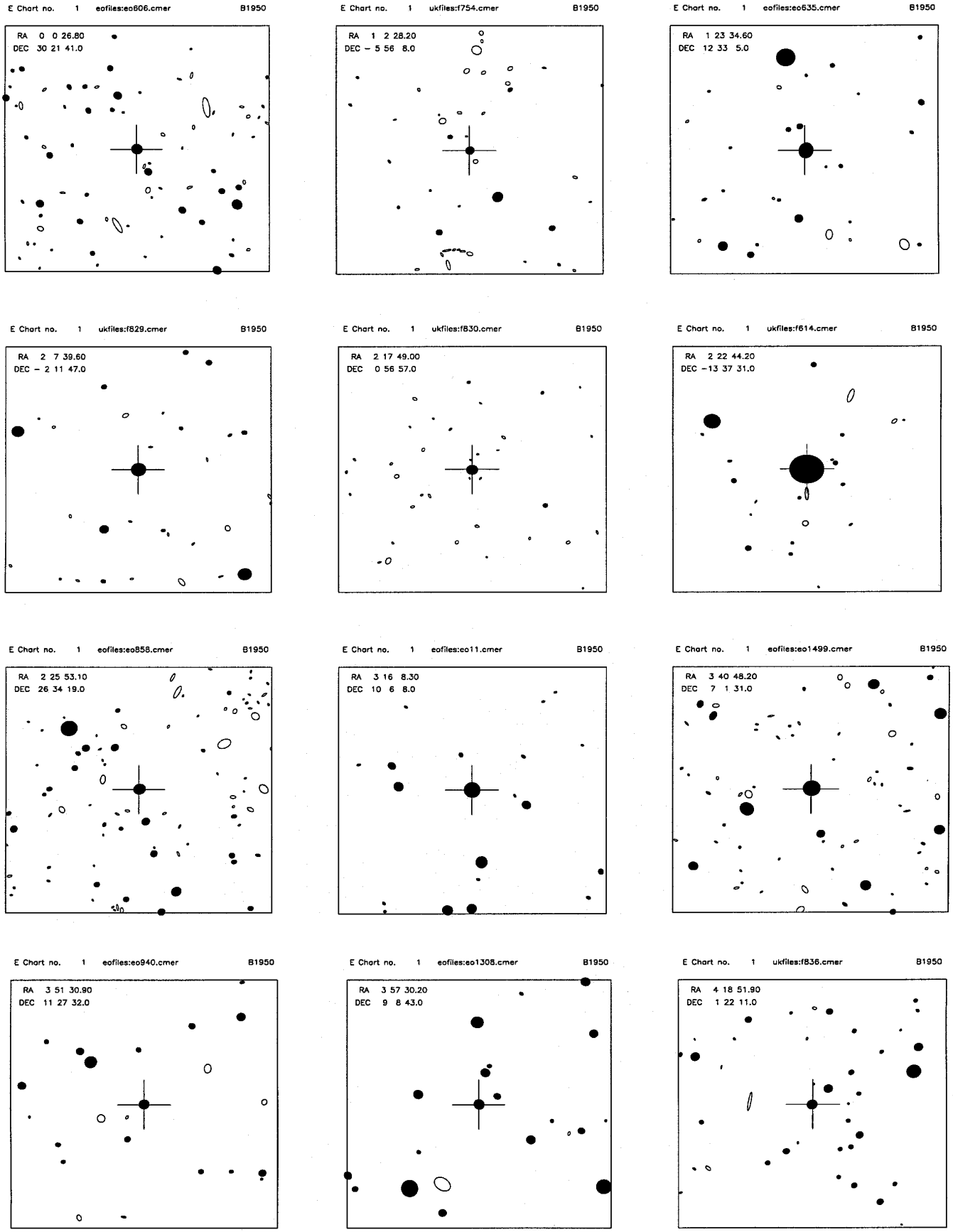

Figure 7. Finding charts for the stars listed in Table 3. Each plot shows a 5×5 arcmin^2 region with north at the top and east to the left. Filled circles are objects classified as stellar; open circles are non-stellar objects.

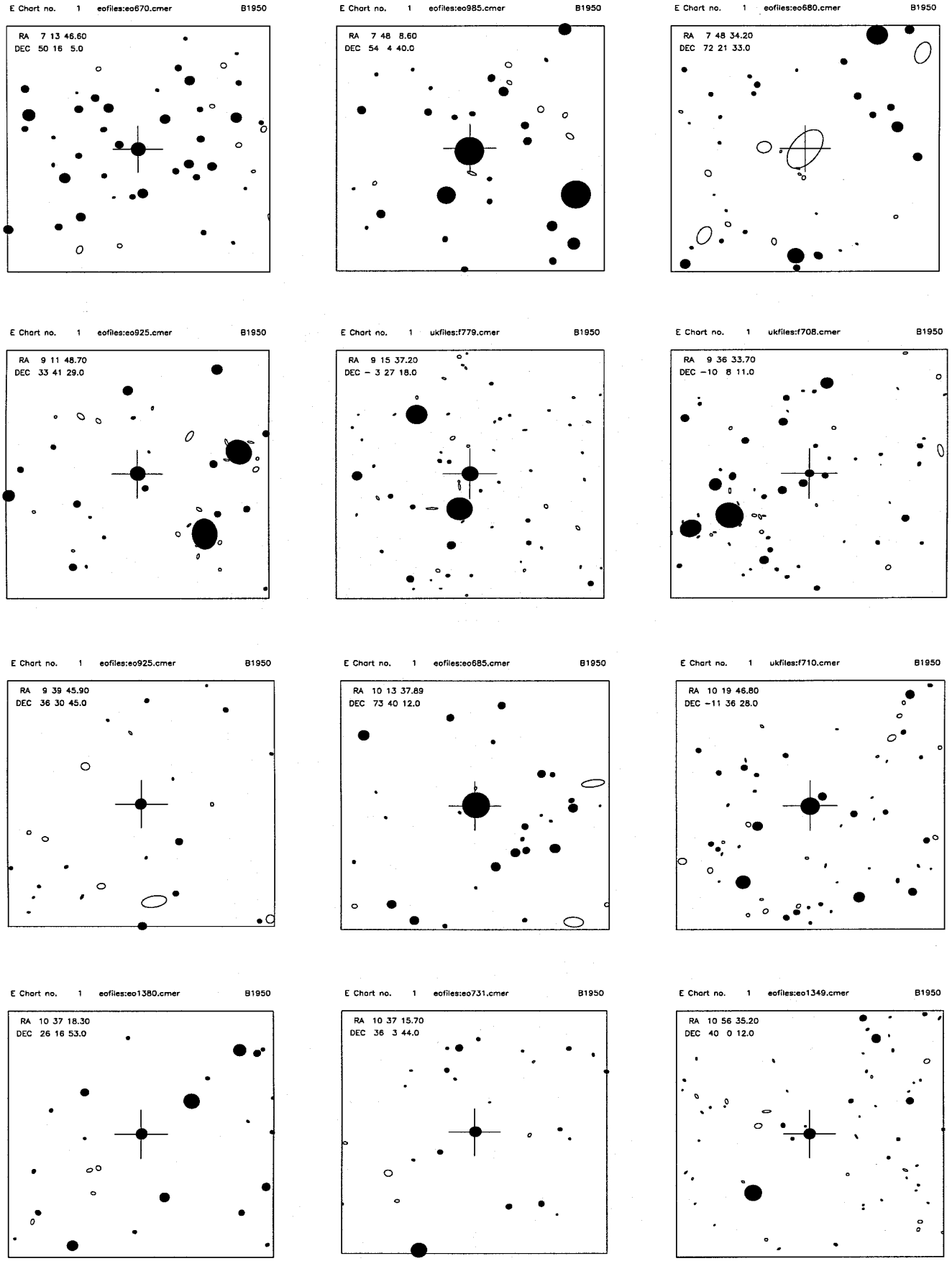

Figure 7 – *continued*

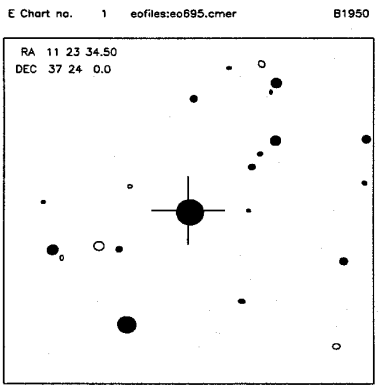

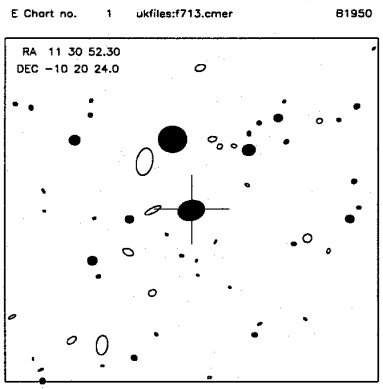

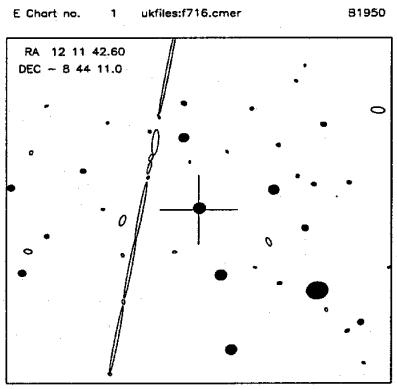

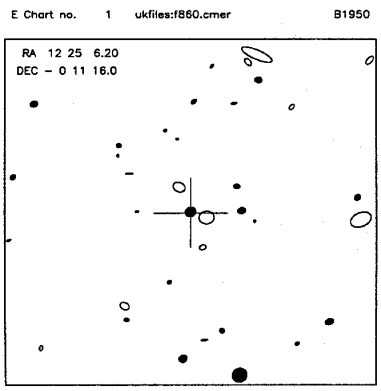

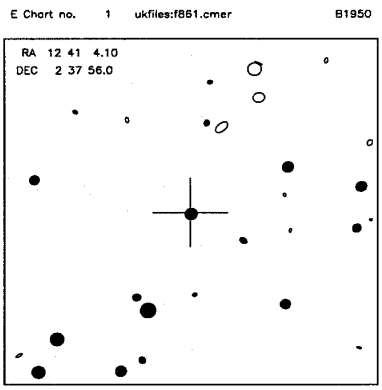

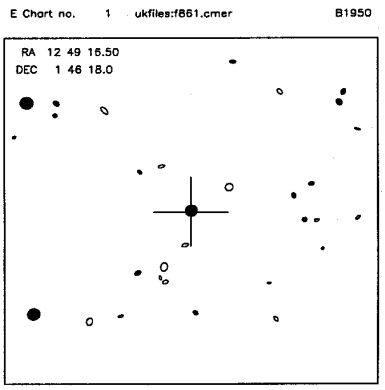

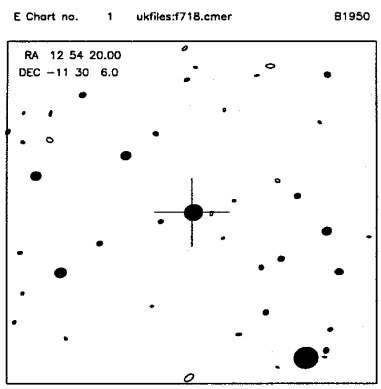

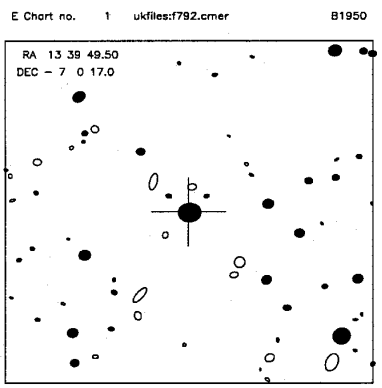

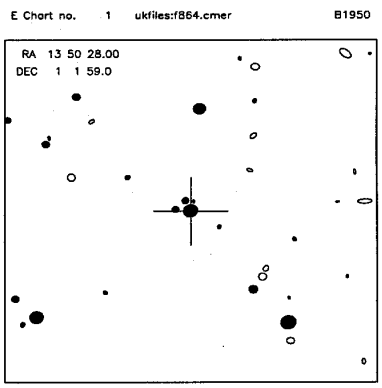

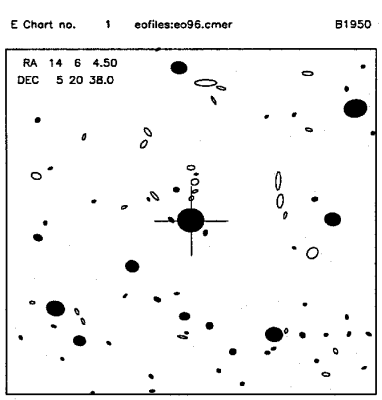

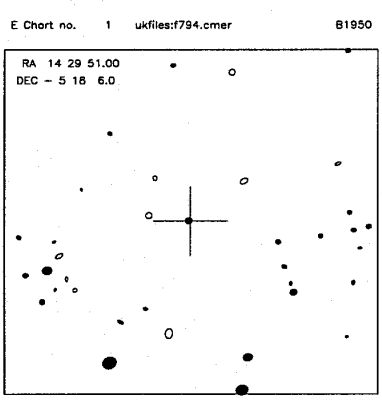

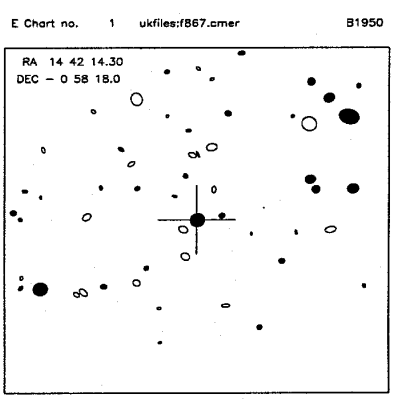

Figure 7 – *continued*

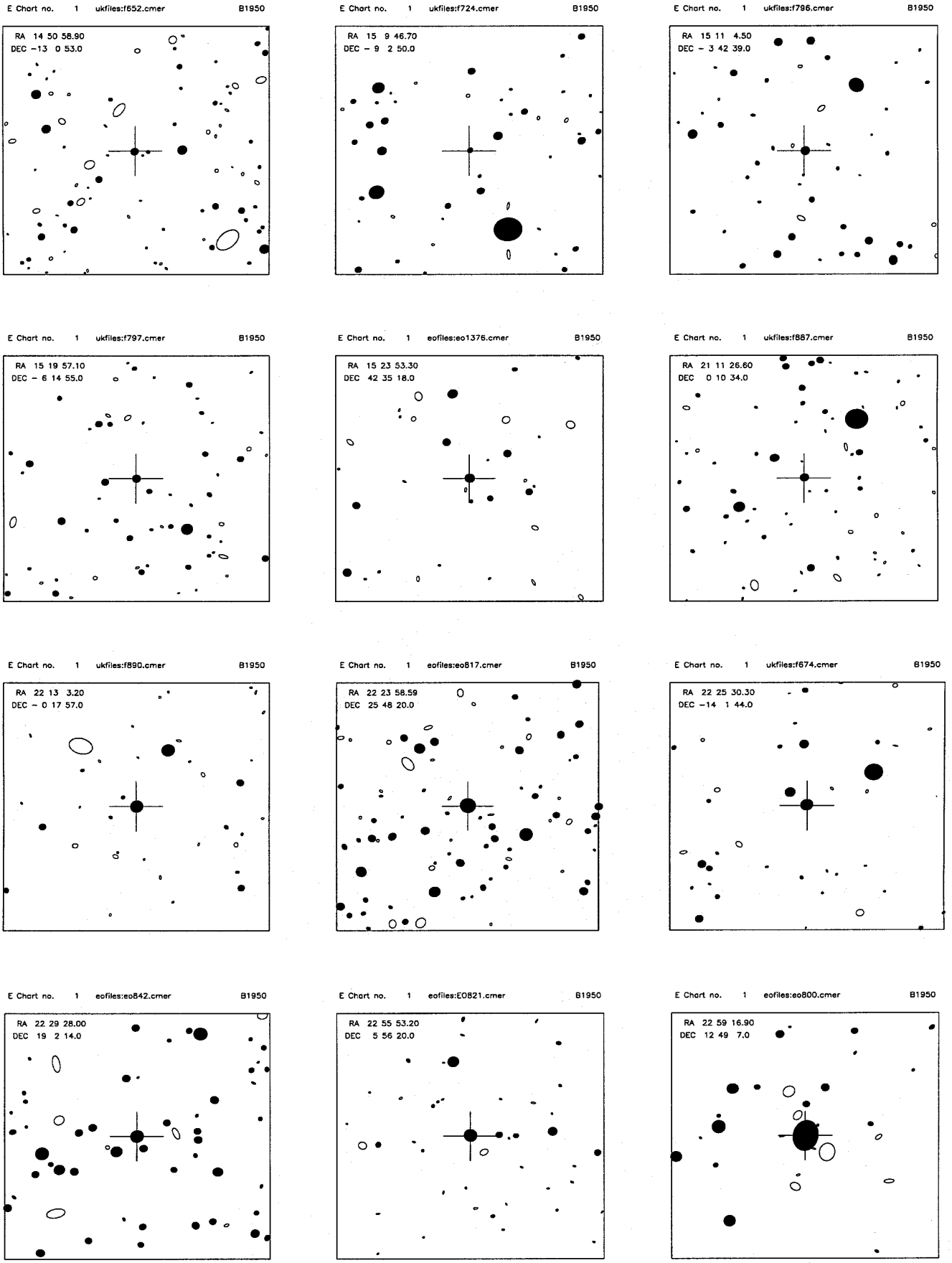

Figure 7 – *continued*

of which agree within the errors with our value of -68 km s^{-1}. The dusty N-type carbon star $1130-1020$ has been observed by Nguyen-Q-Rieu et al., who found a radial velocity of 24 ± 2 km s^{-1}, converted to a heliocentric velocity. Our derived radial velocity is 36 ± 3 km s^{-1} and, taking into account the errors discussed in Section 7.1, these two values are in good agreement. Of the four C* stars in common with Bothun et al., three have velocities that match within the errors quoted by Bothun et al. (±19 km s^{-1}), whilst the fourth, $0102-0556$, differs by some 90 km s^{-1}. This star, C*07, is unusual in that it is one of a few that show Hα in emission (see Fig. 5), indicative of possible chromospheric activity and thence also possible atmospheric velocity variability. The four Case survey stars in common with Bothun et al. (CLS 09, CLS 14 and CLS 38) and Mould et al. (CLS 29) differ by an average of nearly 40 km s^{-1} from the earlier values. This difference is somewhat higher than expected and led us, as a check on our velocity system, to observe recently several carbon stars in common with the survey of the Magellanic Clouds by Demers, Irwin & Kunkel (1993). Our independently derived radial velocities agree to within ±10 km s^{-1} of these velocities.

9.2 Carbon star types

Fluxed spectra for those stars observed in the wavelength range 4100–8600 Å are shown in Fig. 5. Fluxed spectra of those stars only observed in the wavelength range 7500–8600 Å are shown in Fig. 6. We defer a more detailed discussion of the carbon star types to a later paper; however, straightforward inspection of Fig. 5, or from the colours presented in Table 3, reveals the following clear divisions of carbon star type:

$0000+3021$, $0102-0556$, $0207-0211$, $0217+0056$, $0225+2634$, $0340+0701$, $0357+0908$, $0418+0122$, $0748+5404$, $0748+7221$, $0936-1008$, $1013+7340$, $1019-1136$, $1037+2616$, $1056+4000$, $1130-1020$, $1211-0844$, $1225-0011$, $1241+0237$, $1249+0146$, $1254-1130$, $1350+0101$, $1406+0520$, $1429-0518$, $1442-0058$, $1450-1300$, $1511-0342$, $1519-0614$, $1523+4235$, $2213-0017$, $2223+2548$, $2225-1401$, $2229+1902$, $2259+1249$

are N-type carbon stars. As expected, these stars make up the majority of those satisfying the APM survey criteria. Their spectra generally show strong 4737-, 5165- and 5636-Å Swan C_2 bands, although the blue end of the spectrum is often relatively suppressed. Many strong CN bands are also clearly visible around 7000 and 8000 Å – characteristic of cool carbon stars. As expected, the continuum slope is significantly redder in these stars compared with the CH-types, confirming that simple red optical colours can suffice to discriminate between CH- and N-type carbon stars.

As can be seen in the corresponding fluxed spectra in Fig. 5, several of these stars,

$0418+0122$, $1013+7340$, $1130-1020$, $1225-0011$, $2223+2548$

have anomalously red spectra, effectively truncating at ≈5000 Å and with little or no obvious blue C_2 band structure.

A lower resolution spectrum of $1429-0518$ taken during the APM quasar survey shows similar characteristics, which we believe are the signature of enveloping intrinsic dust clouds around these carbon stars. Three of these putative dust-enshrouded carbon stars are in the *IRAS* PSC2.0 catalogue and have *IRAS* fluxes in Jy, as given in Table 5. These fluxes strongly support the likelihood of the presence of copious amounts of dust. The *IRAS* and optical colours of these objects are similar to the two previously discovered dust-enshrouded carbon stars in the halo, $0854+1732$ and $1256+1656$ (see Table 1), and further studies are clearly warranted.

Table 5. *IRAS* flux measurements (Jy).

Carbon Star	12 μ	25 μ	60 μ	100μ
0418+0122	3.37 ± 0.13	1.19 ± 0.11	<0.4	< 1.0
1130−1020	57.37 ± 3.44	21.94 ± 1.54	4.91 ± 0.59	1.39 ± 0.14
2223+2548	11.67 ± 0.58	3.78 ± 0.34	0.65 ± 0.07	< 1.0

$0351+1127$, $0915-0327$, $1339-0700$

are borderline CH-type/N-type, with either the optical colour being close to $B_J-R\approx2.5$ or the optical blue-end spectrum showing tentative, but not conclusive, evidence for a CH absorption band.

$0123+1233$, $0222-1337$, $0316+1006$, $0911+3341$, $0939+3630$, $1037+3603$, $1123+3723$, $1509-0902$, $2111+0010$, $2255+0556$

are CH-type carbon stars. Their spectra as seen in Fig. 5 clearly show the presence of the G band of CH at 4300 Å; they generally have much bluer continua than the N-type stars, and show very strong Swan C_2 bandheads at 4383, 4737, 5165 and 5635 Å. Since these stars make up the majority of the halo carbon star population and the APM colour selection boundary overlaps the CH-type colours, we are not surprised to find some of them within the survey. As noted earlier, most of the N-type carbon stars lie redward of $B_J-R=2.5$, and the majority of CH-type carbon stars lie blueward of this colour.

Several of the N-type carbon stars,

$0102-0556$, $0713+5016$, $1211-0844$, $1523+4235$, $2223+2548$, $2259+1249$,

have obvious Balmer series emission lines present, with Hα being particularly strong in some of them, indicative of possible strong chromospheric activity or shock-waves of the type associated with Mira variables. One of the CH-type carbon stars, $1037+3603=$CLS 29, also has Hα in emission.

9.3 Spatial distribution

The spatial distribution of all the currently known high-latitude distant carbon stars listed in Tables 1 and 3 are shown in an Aitoff projection in Fig. 4. Filled circles are the subset satisfying our colour and magnitude selection criteria. The dashed line denotes the current declination limit of the APM survey, $\delta=-20°$. There is suggestive evidence

for a non-random distribution of carbon stars in both the NGC and SGC samples, as might be expected from the Galaxy merger scenario. However, we caution that the NGC sample is still incomplete. We are currently acquiring *JHK* photometry of all the newly discovered carbon stars to better constrain their distance estimates. Without more accurate distances and fuller spatial coverage, detailed analysis of the phase-space structure of the halo carbon stars is somewhat premature, and we defer this discussion to later work.

ACKNOWLEDGMENTS

This paper is based on observations obtained with the Isaac Newton Telescope operated on the island of La Palma by the Royal Greenwich Observatory in the Spanish Observatorio del Roque de los Muchachos of the Institudo de Astrophysica de Canarias. We gratefully acknowledge the UKST unit for providing the excellent plate material essential to the APM survey. The APM is a National Astronomy Facility, at the Institute of Astronomy, run by the Royal Greenwich Observatory. Thanks are also due to the past and present members of the APM facility for producing and maintaining such an excellent system, to Paul Green for his advice and encouragement on carbon star surveys, and to the service programme run by the La Palma observatory. We thank an anonymous referee for constructive comments and suggestions. EJT is grateful for a Department of Education for Northern Ireland CAST Research Studentship held jointly at Queen's University, Belfast and at the Royal Greenwich Observatory, Cambridge.

REFERENCES

Abramyan G.V., Gigoyan K. S., 1993, Afz, 36, 181
Azzopardi M., Lequeux J., 1992, in Barbuy B., Renzini A., eds, The Stellar Populations of Galaxies. Kluwer, Dordrecht, p. 201
Beichman C. A. et al., 1990, AJ, 99, 1569
Bothun G. et al., 1991, AJ, 101, 2220
Bunclark P. S., Irwin M. J., 1983, in Proc. Statistical Methods in Astronomy. ESA SP-201, p. 195
Cutri R. M. et al., 1989, AJ, 97, 866
Dahn C. C. et al., 1977, ApJ, 216, 757
Demers S., Irwin M. J., 1987, MNRAS, 226, 943
Demers S. et al., 1986, AJ, 92, 878
Demers S., Irwin M. J., Kunkel W. E., 1993, MNRAS, 260, 103
Deutsch E. W., 1994, PASP, 106, 1134
Evans D., 1988, PhD thesis, Univ. Cambridge
Feast M. W., Whitelock P. A., 1992, MNRAS, 259, 6
Green P. J., Margon B., MacConnell D. J., 1991, ApJ, 380, 30
Green P. J. et al., 1992, ApJ, 400, 659
Green P. J. et al., 1994, ApJ, 433, 319
Harding G. A., 1962, Observatory, 82, 205
Hartwick F. D., Cowley A. P., 1991, in Haynes R., Milne D., eds, Proc. IAU Symp. 148, The Magellanic Clouds. Kluwer, Dordrecht, p. 77
Heber U. et al., 1993, A&A, 267, 31
Ibata R., Gilmore G., Irwin M. J., 1994, Nat, 370, 194
Irwin M. J., 1991, in Haynes R., Milne D., eds, Proc. IAU Symp. 148, The Magellanic Clouds. Kluwer, Dordrecht, p. 453
Irwin M. J., 1993, in Meylan G., Prugniel P., eds, ESO/OHP Workshop No 49 on Dwarf Galaxies. ESO, Garching, p. 27
Irwin M. J., McMahon R., 1992, Gemini, 36, 1
Irwin M. J., Demers S., Kunkel W. E., 1990, AJ, 99, 191
Irwin M. J., McMahon R. G., Hazard C., 1991a, in ASP Conf. Ser. Vol. 21, Density of Quasars. Astron. Soc. Pac., San Francisco, p. 117
Irwin M. J., McMahon R. G., Reid N., 1991b, MNRAS, 252, 61P
Irwin M. J., Maddox S. J., McMahon R., 1994, Spectrum No. 2, p. 14
Johnston K. et al., 1996, in Morrison H., Sarajedini A., eds, ASP Conf. Ser. Vol. 92, Formation of the Galactic Halo ... Inside and Out. Astron. Soc. Pac., San Francisco, p. 483
Jones B. F., Klemola A. R., Lin D. N. C., 1994, AJ, 107, 1333
Keenan P. C., 1993, PASP, 105, 905
Kibblewhite E. J. et al., 1984, in Klinglesmith D. A., ed., Proc. Astronomical Microdensitometry Conference. NASA-2317, p. 277
Kunkel W. E., Demers S., 1976, Greenwich Obs. Bull., 182, 241
Kunkel W. E., Demers S., Irwin M. J., 1997, A&AS, 122, 463
Lasker B. M. et al., 1988, ApJS, 68, 1
Liebert J. et al., 1994, ApJ, 421, 733
Lynden-Bell D., 1976, MNRAS, 174, 695
Lynden-Bell D., Lynden-Bell R. M., 1995, MNRAS, 275, 429
MacAlpine G. M., Lewis D., 1978, ApJS, 36, 587
Majewski S. R., 1994, ApJ, 431, L17
Margon B. et al., 1984, AJ, 89, 274
Mathewson D. S., Cleary M. N., Murray J. D., 1974, ApJ, 190, 291
McClure R. D., 1979, Mem. Soc. Astron. Ital., 50, 15
Mould J. R. et al., 1985, PASP, 97, 130
Nguyen-Q-Rieu et al., 1987, A&A, 180, 117
Oh K. S., Lin D. N. C., Aarseth S. J., 1995, ApJ, 442, 142
Phillips M., Terlevich R., 1983, PASP, 95, 43
Richer H. B., Westerlund B. E., 1983, ApJ, 264, 114
Rodgers A., Paltoglou G., 1984, ApJ, 283, L5
Roeser S., Bastian U., 1988, A&AS, 74, 449
Saha A., 1985, ApJ, 289, 310
Sanduleak N., 1980, PASP, 92, 246
Sanduleak N., Pesch P., 1982, PASP, 94, 690
Sanduleak N., Pesch P., 1988, ApJS, 66, 387
Sanduleak N., Philip A. G. D., 1977, Publ. Warner & Swasey Obs., Vol. 1, No. 5
Searle L., Zinn R., 1978, ApJ, 225, 357
Stephenson C. B., 1989, Publ. Warner & Swasey Obs., Vol. 3, No. 2
Toomre A., Toomre J., 1972, ApJ, 178, 623
Tremaine S., 1976, ApJ, 203, 72
Unavane M., Wyse R., Gilmore G., 1996, MNRAS, 278, 727
van den Bergh S., Lafontaine A., 1984, PASP, 96, 869
Warren S. J. et al., 1993, MNRAS, 261, 185
Westerlund B. E. et al., 1986, A&AS, 65, 79